

Compositional data analysis and geochemical modeling of CO₂–water–rock interactions in three provinces of Korea

Seong Hee Kim · Byoung-Young Choi · Gyemin Lee · Seong-Taek Yun · Soon-Oh Kim

Received: 25 September 2017 / Accepted: 12 December 2017 / Published online: 20 December 2017
© Springer Science+Business Media B.V., part of Springer Nature 2017

Abstract The CO₂-rich spring water (CSW) occurring naturally in three provinces, Kangwon (KW), Chungbuk (CB), and Gyeongbuk (GB) of South Korea was classified based on its hydrochemical properties using compositional data analysis. Additionally, the geochemical evolution pathways of various CSW were simulated via equilibrium phase modeling (EPM) incorporated in the PHREEQC code. Most of the CSW in the study areas grouped into the Ca–HCO₃ water type, but some samples from the KW area were classified as Na–HCO₃ water. Interaction with anorthite is likely to be more important than interaction with carbonate minerals for the hydrochemical properties of the CSW in the three areas, indicating that the

CSW originated from interactions among magmatic CO₂, deep groundwater, and bedrock-forming minerals. Based on the simulation results of PHREEQC EPM, the formation temperatures of the CSW within each area were estimated as 77.8 and 150 °C for the Ca–HCO₃ and Na–HCO₃ types of CSW, respectively, in the KW area; 138.9 °C for the CB CSW; and 93.0 °C for the GB CSW. Additionally, the mixing ratios between simulated carbonate water and shallow groundwater were adjusted to 1:9–9:1 for the CSW of the GB area and the Ca–HCO₃-type CSW of the KW area, indicating that these CSWs were more affected by carbonate water than by shallow groundwater. On the other hand, mixing ratios of 1:9–5:5 and 1:9–3:7 were found for the Na–HCO₃-type CSW of the KW area and for the CSW of the CB area, respectively, suggesting a relatively small contribution of carbonate water to these CSWs. This study proposes a systematic, but relatively simple, methodology to simulate the formation of carbonate water in deep environments and the geochemical evolution of CSW. Moreover, the proposed methodology could be applied to predict the behavior of CO₂ after its geological storage and to estimate the stability and security of geologically stored CO₂.

S. H. Kim · S.-O. Kim (✉)
Department of Geology and Research Institute of Natural Science (RINS), Gyeongsang National University (GNU), Jinju, Republic of Korea
e-mail: sokim@gnu.ac.kr

B.-Y. Choi
Center for CO₂ Geological Storage, Korea Institute of Geoscience and Mineral Resources (KIGAM), Daejeon, Republic of Korea

G. Lee
Department of Information and Statistics and Research Institute of Natural Science (RINS), Gyeongsang National University (GNU), Jinju, Republic of Korea

S.-T. Yun
Department of Earth and Environmental Sciences, Korea University, Seoul, Republic of Korea

Keywords CO₂-rich spring water · CO₂–water–rock interaction · Compositional data analysis · Equilibrium phase modeling · Geological CO₂ storage

Introduction

Remarkable technological and industrial growth has been achieved through the use of fossil fuels; however, this has also led to the emission of large quantities of greenhouse gases such as carbon dioxide (CO₂) into the atmosphere, resulting in environmental disasters such as acid rain and global warming. Carbon dioxide geological storage (CGS) has been considered as one effective technology for mitigation of the detrimental effects of CO₂. However, because CGS technology injects CO₂ into deep subsurface environments, a range of minerals such as silicates and carbonates can be dissolved and/or precipitated as a result of changes in groundwater properties. Such water–rock interactions might occur over a long time span; however, our knowledge of these processes is limited due to the relatively recent adoption of CGS technology (Kharaka et al. 2006; Gaus 2010). For this reason, natural analogue studies using CO₂-rich spring water (CSW) have been conducted to advance our knowledge of CGS-driven geochemical processes over geological timescales (Watson et al. 2004; Moore et al. 2005; Pearce 2006; Pauwels et al. 2007; Flaathen et al. 2009; Lu et al. 2011; Choi et al. 2012, 2014; Chopping and Kaszuba 2012).

There have been a number of studies using naturally occurring CSW that have investigated relatively long-term geochemical processes in deep groundwaters after CO₂ injection (Balashov et al. 2013, 2015). CSW is most frequently observed in South Korea in the Kangwon (KW), Chungbuk (CB), and Gyeongbuk (GB) districts. The main geology where CSW occurs is granite and banded gneiss for the KW area, granite and alluvial deposits for the CB province, and sedimentary deposits for the GB region (Bong and Chung 2000; Lee et al. 2003; Yun et al. 2003; Noh et al. 2004; Hwang et al. 2013). Previous studies have compared the properties of CSW between areas and investigated the origin and evolutionary pathway of CSW using isotope studies (Koh et al. 1999, 2000, 2008; Choi et al. 2000, 2002, 2005, 2009; Jeong and Lee 2000; Kim et al. 2000, 2001, 2008; Yun and Kim 2000; Jeong 2002, 2004; Jeong et al. 2001, 2005, 2011; Chae et al. 2013). Although the isotope composition of specific elements has been used to investigate the origin and evolutionary pathways of CSW, such approaches are not appropriate for characterizing water–rock interactions resulting from

the carbonate water produced in deep subsurface environments on CSW occurring on the surface. Instead, a number of studies have attempted to understand the water–rock interactions using geochemical modeling. Choi et al. (2014) studied the geochemical pathways of two types (Na–HCO₃ and Ca–HCO₃) of CSW in the GW district using geochemical (reaction path) modeling, including mixing and ion-exchange reactions. Additionally, there have been many attempts to calculate the saturation indices of minerals within carbonate aquifers using equilibrium reaction modeling (Zanini et al. 2000; Kharitonova et al. 2010; Akin et al. 2015; Jin et al. 2015; Nyirenda et al. 2015).

There are two types of approaches for using multivariate statistical analyses with hydrogeochemical data. One is to use traditional statistical techniques, and the other is to use compositional data analysis. Despite being commonplace, traditional techniques cannot treat the data as compositional data and implicitly invoke spurious correlations caused by scaling because they employ amalgamation, which does not preserve distances within an already restricted sample space (called the simplex) (Egozcue and Pawlowsky-Glahn 2005; Bacon-Shone 2006; Pawlowsky-Glahn and Egozcue 2006; Owen et al. 2016). This occurs because hydrochemical data are compositional by nature; in particular, they are quantitative data in which each component is a proportion of a given total (Owen et al. 2016). Compositional data refer to data in which the relevant information is contained in the ratios between the values of the variables. Aitchison (1986) introduced log ratio approaches, such as additive log ratios (alt) and centered log ratios (clr), to treat compositional data in percentages, proportions, concentrations, etc. (Filzmoser et al. 2016). More recently, the isomeric log ratio (ilr) approach was developed, which ultimately led to recognition that compositions can be represented in orthogonal (Cartesian) coordinates in the simplex (Egozcue and Pawlowsky-Glahn 2005; Owen et al. 2016). Collectively, these methods are called compositional data analysis. Recently, there have been several applications of compositional data analyses in the fields of geochemistry and hydrogeochemistry (Blake et al. 2016; Buccianti and Zuo 2016; Tolosana-Delgado and McKinley 2016). Fačevićová et al. (2016) reported a statistical characterization of the Devonian–Carboniferous boundary, in which

results obtained by a log ratio method were compared with those obtained from a classical point of view, without any prior transformation. The paper proposed that using a combination of the two approaches brings more insights than using either of any of the two methods separately. Furthermore, Owen et al. (2016) applied compositional data analysis techniques to describe the variability of major ions within and between coal seam gas-bearing (or coal bed methane-bearing) groundwater. Using the compositional data analysis, they described fundamental compositional similarities/differences between coal seam gas and groundwater, provided a robust and descriptive means of comparing water types, and assessed hydrochemical variability within and between large and highly variable datasets with respect to the hydrochemical evolution of coal seam gas or groundwater associated with high gas concentrations.

Equilibrium phase modeling (EPM) can be used to target the solid, liquid, and gas phases and has been actively used to compute a variety of aqueous chemical reactions in equilibrium. In particular, EPM has recently been used in numerous CGS and natural analogue studies of carbonate water and CSW. Springer et al. (2012) conducted a study using EPM to simulate the dissolution of CO_2 according to the temperature and pressure of the saline aquifer in which a CGS project had been implemented. In addition, Bollengier et al. (2013) performed an EPM study to estimate phase changes of water and CO_2 at a specific temperature and pressure and to evaluate the stability of CO_2 hydrates in deep sea environments. EPM was used to investigate chemical equilibrium reactions taking place in the groundwater of karst regions (White 1997) and to observe the phase changes of carbon in deep groundwater aquifers when magmatic CO_2 moved up from the upper mantle (Manning et al. 2013). EPM has also been used in numerous laboratory studies to simulate diverse carbonate water and groundwater environments (Evans and Derry 2002; Garcia-Rios et al. 2014; Martos-Rosillo and Moral 2015; Raju et al. 2015). However, EPM is not likely to be reliable when it is applied to a wide study area or large datasets. To overcome such drawbacks, multivariate statistical analysis can be used in conjunction with EPM when geochemical modeling is applied in groundwater studies (Sharif et al. 2008; Belkhir et al. 2010; Ryzhenko and Cherkasova 2012; Tallini et al.

2014; Ledesma-Ruiz et al. 2015; Sanchez et al. 2015; Rafighdoust et al. 2016).

Even though there have been a number of studies of CSW in South Korea, most have been limited to a local area. The lack of an overall understanding of CSW on a national scale motivated this study. The objectives of this study were therefore: (1) to compare the hydrochemical properties of CSW occurring in three typical districts in South Korea and (2) to determine the evolutionary pathways of carbonate water and CSW. To achieve these objectives, compositional data analyses and geochemical modeling were utilized. In particular, past geochemical processes in CSW were described by EPM to interpret the carbonate water–rock interactions arising in subsurface environments and relate them to the occurrence of surface CSW.

Geology of the study area

The typical areas where CSW occurs in South Korea are in the KW, CB, and GB provinces. The geology of these areas and the location of CSW sampling sites are given in Fig. 1. The KW province is located in northeastern South Korea and predominantly consists of Precambrian metamorphic rocks, including porphyroblastic, banded, and leucocratic gneisses, together with Jurassic biotite granites and sedimentary rocks (Yun and Kim 2000; Choi et al. 2014). The dominant mineral composition in this area is quartz (33.4%), albite (24.5%), K-feldspar (21.5%), anorthite (11.3%), biotite (3.8%), and hematite (2.8%), with minor components of magnetite, muscovite, and pargasite (Choi et al. 2014). The main geology of the KW area, where CSWs of Na-HCO_3 type frequently occur, has been reported to be Cretaceous Bulguksa granite, which has a mineralogy of albite (35.4%), quartz (30.1%), K-feldspar (26.7%), anorthite (2.2%), magnetite (1.2%), ferrosilite (0.1%), and enstatite (0.1%) (Min and Kim 1996). The CB province, located in central South Korea, mainly consists of Precambrian gneisses and Jurassic granites extending to the KW province, with minor components of Paleozoic metamorphic sedimentary rocks (Jeong et al. 2001; Koh et al. 2008). The main mineral composition of the CB area is quartz (27.4%), plagioclase (38.0%), K-feldspar (26.3%), biotite (6.2%), and muscovite (1.6%), with some calcite and pargasite (Koh et al. 2008). The GB province is located in eastern South

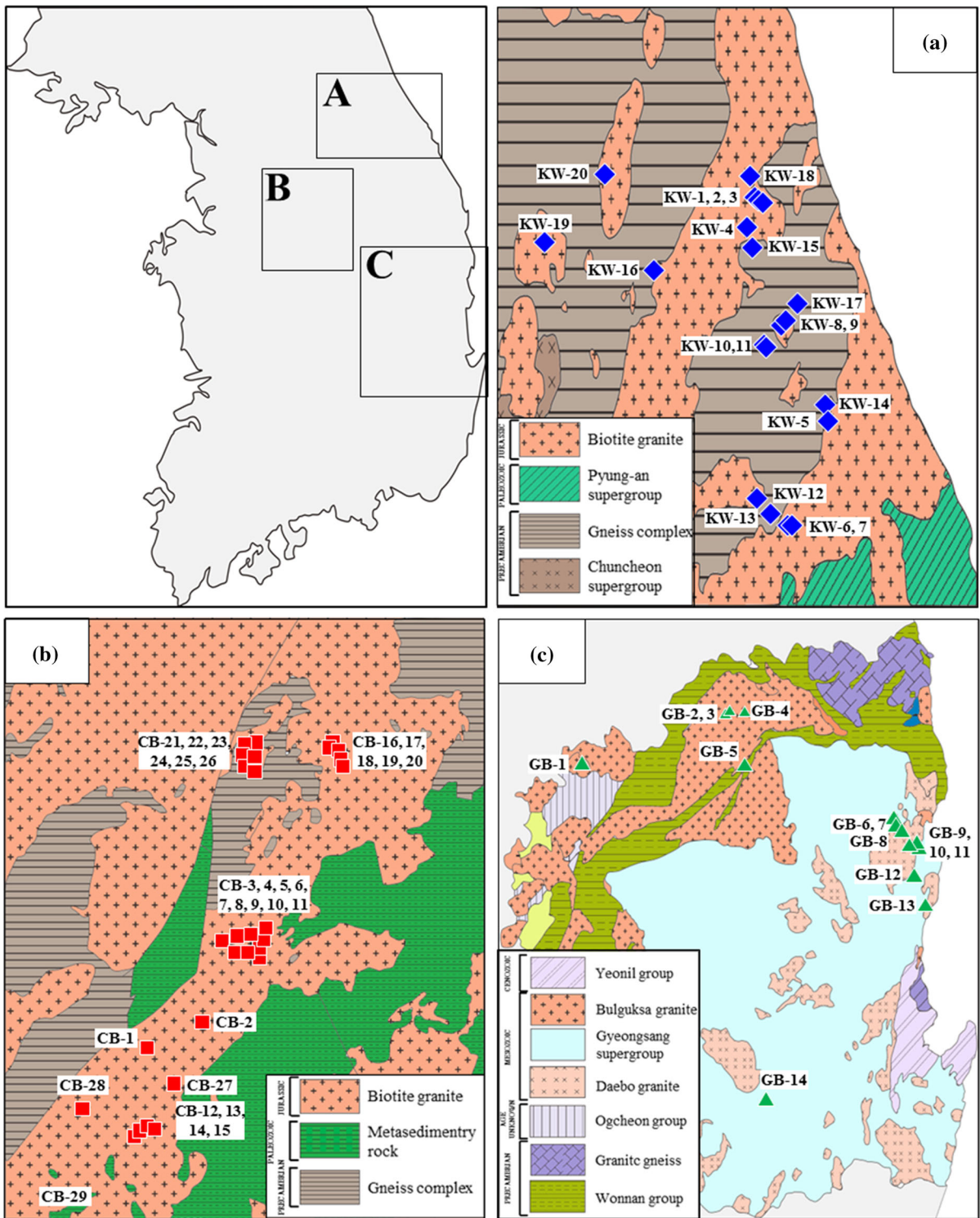


Fig. 1 Geological map of the study area with the locations of CO₂-rich spring water (CSW). **a** Kangwon (KW) area, **b** Chungbuk (CB) area and **c** Gyeongbuk (GB) area

Korea. The main geology of the GB area is Jurassic sedimentary and Cretaceous granitic rocks (Yun and Kim 2000). Lee and Lee (1991) conducted petrological research on the granite of the GB area and reported that the main mineralogy of this area was quartz (27.9%), plagioclase (44.5%), biotite (12.9%), K-feldspar (11.4%), epidote (1.8%), ripidolite (0.6%), and pargasite (0.3%). In addition, Jeong and Jeong (1999) studied the sedimentary rocks conformably or unconformably covering granitic rocks within the GB area and reported that the mineralogy of the sedimentary rocks was quartz (33.4%), plagioclase (22.8%), K-feldspar (5.2%), muscovite (0.6%), and carbonate minerals including calcite and dolomite (36.9%).

Methodology

Data collection and processing

For this study, we investigated a number of previous studies of CSW undertaken within the three districts and collected CSW hydrochemical data from 54 sites. The data were classified into three groups: (1) on-site measurements such as pH, temperature, electrical conductivity (EC), and total dissolved solid (TDS), (2) major constituents such as cations (Na, Ca, K, and Mg) and anions (Cl, HCO₃, SO₄, and NO₃), and (3) minor elements (Al, Fe, and Si). Data collection was restricted because the analytical items were different between studies, and for this reason, the use of dissolved oxygen (DO) and oxidation–reduction potential (ORP) data was excluded in this study. It was possible to acquire analytical data on major ion constituents from most previous studies, whereas data on minor elements differed significantly between studies, and only three elements (Al, Fe, and Si) commonly analyzed in previous studies were collected and used. In terms of EC and TDS, when only one item was acquired from the literature, the other was calculated using a first-order equation ($y = ax + b$) because the relationship between them is commonly assumed to be linear. The data acquired from the literature are summarized in Tables 1 and 2. The CSW hydrochemical data were also characterized by Piper diagrams, ternary principal components plots, and relationships between molar ratios of major constituents and TDS/HCO₃.

Compositional data analyses

To statistically interpret the CSW data collected from the literature, a total of 12 parameters (pH, Na, Ca, K, Mg, HCO₃, Cl, SO₄, NO₃, Al, Fe, and Si) were used for the statistical analyses. pH values were converted to hydrogen (H⁺) ion concentrations in mg/L to match the unit with that of the other variables.

Compositional data have several weaknesses for direct application of conventional multivariate statistical analysis, e.g., spurious correlation (Pearson 1896). For this reason, compositional data analyses were conducted using R package (v. 3.3.2), CodaPack (v. 2.02.04), and IBM® SPSS (v. 22) programs. In this work, two log ratios were applied when analyzing the dataset: (1) *D*-dimensional centered log ratio (clr) coordinates $[\log \frac{x_1}{(x_1 \cdots x_p)^{1/D}}, \dots, \log \frac{x_p}{(x_1 \cdots x_D)^{1/D}}]$ of *D*-dimensional original data (x_1, \dots, x_D) and (2) the $(D - 1)$ -dimensional isomeric log ratio (ilr) coordinates

$$\left(\sqrt{\frac{r_1 s_1}{r_1 + s_1}} \log \frac{\left(\prod_{+ \in B_{D-1}} x_i\right)^{1/r_1}}{\left(\prod_{- \in B_{D-1}} x_i\right)^{1/s_1}}, \dots, \sqrt{\frac{r_{D-1} s_{D-1}}{r_{D-1} + s_{D-1}}} \log \frac{\left(\prod_{+ \in B_{D-1}} x_i\right)^{1/r_{D-1}}}{\left(\prod_{- \in B_{D-1}} x_i\right)^{1/s_{D-1}}} \right),$$

where B_i is the *i*th sequential binary partition and r_i and s_i are the number of parts coded in B_i as + and –, respectively (Wickham 2009; Owen et al. 2016). Sequential binary partitions define $D - 1$ orthonormal coordinates (ilr coordinates), called balances, which can be modeled by standard statistical methods (Egozcue et al. 2003). The clr transformation produces *D* coordinates, which are useful for constructing biplots to describe variability (Egozcue et al. 2003; Pawlowsky-Glahn and Egozcue 2006). However, the clr-transformed coordinates are constrained to a subspace of real space and are represented on a hyperplane in *D*-dimensional real space because they ultimately sum to zero; consequently, the covariance and correlation matrices are singular (Egozcue et al. 2003; Pawlowsky-Glahn and Egozcue 2006). Therefore, care should be needed during the interpretation of clr-transformed data because the clr-coordinates represent the proportion in the numerator concerning the

Table 1 Physical and chemical data of CO₂-rich spring water (CSW) used in this study

Sample ID	Temp. (°C)	pH	EC (μS/cm)	TDS (mg/l)	Sample ID	Temp.(°C)	pH	EC (μS/cm)	TDS (mg/l)
KW-1 ^a	18.5	6.2	4533*	1773	CB-9 ^c	15.0	5.8	670.0	294.4*
KW-2 ^a	18.2	6.2	6756*	2625	CB-10 ^c	16.4	5.6	663.0	291.7*
KW-3 ^a	11.2	6.6	4000*	1569	CB-11 ^c	21.2	5.4	354.0	172.2*
KW-4 ^a	9.80	6.7	4987*	1947	CB-12 ^c	16.6	5.0	138.0	88.60*
KW-5 ^a	1.50	5.7	1422*	581.0	CB-13 ^c	14.2	5.0	146.0	91.70*
KW-6 ^a	17.6	5.9	2824*	1118	CB-14 ^c	15.2	4.9	128.0	84.80*
KW-7 ^a	13.5	6.5	2429*	967.0	CB-15 ^c	14.5	4.8	101.0	74.30*
KW-8 ^a	14.4	6.0	3726*	1464	CB-16 ^c	25.9	6.4	1857	753.5*
KW-9 ^a	13.3	5.5	999.9*	419.0	CB-17 ^c	27.5	6.8	2820	1126*
KW-10 ^a	10.7	5.9	1581*	642.0	CB-18 ^c	25.4	6.7	2950	1176*
KW-11 ^a	7.30	6.3	5107*	1993	CB-19 ^c	24.3	6.5	1856	753.1*
KW-12 ^a	7.40	6.3	2450*	975.0	CB-20 ^c	30.7	6.8	2790	1114*
KW-13 ^a	4.70	5.5	2513*	999.0					
KW-14 ^a	14.1	5.8	2082*	834.0	GB-1 ^d	25.8	6.4	1705	694.7*
KW-15 ^a	12.4	5.5	2884*	1141	GB-2 ^d	13.4	5.3	422.0	198.5*
KW-16 ^b	6.30	6.0	2911*	1151	GB-3 ^d	11.5	5.3	559.0	251.5*
KW-17 ^b	3.70	6.0	1569*	1413	GB-4 ^d	3.90	5.2	1391	573.3*
KW-18 ^b		6.0	1959*	1763	GB-5 ^d	11.3	5.4	988.0	417.4*
KW-19 ^b	6.30	6.1	3063*	1209	GB-6 ^d	8.20	5.2	625.0	277.0*
KW-20 ^b	5.00	6.3	2828*	1119	GB-7 ^d	12.9	5.8	1520	623.2*
					GB-8 ^d	10.1	5.7	1156	482.4*
CB-1 ^c	13.6	6.0	1674	682.7*	GB-9 ^d	7.90	5.6	1452	596.9*
CB-2 ^c	13.6	5.9	436.0	203.9*	GB-10 ^d	8.60	5.8	908.0	386.5*
CB-3 ^c	15.5	5.3	491.0	225.2*	GB-11 ^d	10.8	5.6	1442	593.0*
CB-4 ^c	18.5	5.8	1265	524.5*	GB-12 ^d	14.0	5.9	2280	917.1*
CB-5 ^c	16.2	5.5	563.0	253.0*	GB-13 ^d	11.2	6.4	1736	706.7*
CB-6 ^c	15.0	5.4	489.0	224.4*	GB-14 ^d	16.7	6.2	1045	439.5*
CB-7 ^c	16.1	5.4	556.0	250.3*					
CB-8 ^c	17.7	5.6	390.0	186.1*					

*Calculated value

^aChoi et al. (2005)^bYun and Kim (2000)^cJeong et al. (2001)^dJeong (2002)

geometric mean of all the parts in the composition (Owen et al. 2016). We used the information derived from the biplot to develop meaningful sequential binary partitions for *ilr* transformation. Finally, a hierarchical cluster analysis (HCA) based on Euclidean square distance and Ward linkage was applied to the *ilr* coordinates. This method of performing an HCA means that the clustered groups represent

compositional similarities in the simplex, rather than simply similarities in individual ion concentrations. Before applying the procedures described above, the data below the detection limit (typically NO₃ and Al) were imputed using the log ratio data augmentation function (*lrDA*) in the R package *zCompositions*, which is a function based on the log ratio Markov chain Monte Carlo data augmentation (DA) algorithm

Table 2 Elemental concentrations of CO₂-rich spring water (CSW) used in this study (unit: mg/L)

	Na	Ca	K	Mg	HCO ₃	Cl	NO ₃	SO ₄	Fe	Al	Si
KW-1 ^a	419.0	44.60	25.0	2.10	1159	8.30	0.07*	13.8	5.20	0.30	87.7
KW-2 ^a	544.0	57.10	32.1	2.60	1861	2.50	0.08*	22.4	2.10	0.10	93.1
KW-3 ^a	408.1	12.90	5.70	0.30	1052	4.40	0.07*	3.70	3.30	0.10	73.7
KW-4 ^a	488.4	46.30	7.60	4.00	1334	8.10	0.06*	6.10	1.20	0.10	48.1
KW-5 ^a	64.60	58.30	2.80	5.90	386.0	10.8	0.03*	14.1	5.40	0.40	28.7
KW-6 ^a	113.0	152.0	3.80	21.3	750.0	20.9	0.08*	13.2	1.60	0.10	38.1
KW-7 ^a	89.70	134.2	2.40	11.9	656.0	11.2	0.09*	7.90	5.70	3e−4*	37.5
KW-8 ^a	32.30	293.8	4.20	25.7	988.0	2.90	0.08*	21.1	16.3	1e−3*	76.1
KW-9 ^a	6.600	72.50	0.50	9.70	249.0	3.30	0.10*	13.6	6.60	0.50	54.0
KW-10 ^a	15.00	109.7	2.70	11.9	411.0	2.60	0.10*	10.5	14.3	0.50	60.8
KW-11 ^a	49.10	348.7	2.40	45.9	1434	5.90	0.08*	12.3	16.3	0.10	73.4
KW-12 ^a	32.60	178.3	2.50	16.2	702.0	2.70	0.10*	3.90	8.80	4e−4*	24.9
KW-13 ^a	15.00	138.0	1.20	37.4	735.0	5.80	0.09*	8.60	17.1	0.10	38.7
KW-14 ^a	15.20	93.00	2.90	46.1	610.0	2.10	0.09*	7.60	25.5	1e−3*	30.2
KW-15 ^a	35.90	198.1	3.30	20.9	808.0	2.90	0.05*	8.20	12.4	4e−3*	48.4
KW-16 ^b	18.60	130.0	11.2	74.0	863.3	4.40	0.08*	2.30	17.1	0.02	28.3
KW-17 ^b	29.20	269.0	4.10	21.4	1013	4.10	0.09*	23.1	16.9	0.04	30.7
KW-18 ^b	400.0	41.90	37.0	0.28*	1204	9.20	0.09*	22.9	4.80	1.14	36.9
KW-19 ^b	37.50	226.0	3.70	8.40	870.8	4.30	0.06*	6.50	23.8	0.62	22.3
KW-20 ^b	20.40	229.0	7.40	8.20	808.0	3.50	0.07*	5.60	8.90	0.08	26.8
CB-1 ^c	73.10	293.0	2.80	19.5	1221	4.60	0.10	8.70	13.2	0.10	34.5
CB-2 ^c	43.50	39.70	3.10	8.80	241.0	15.0	0.10	21.6	2.51	0.06	9.40
CB-3 ^c	28.70	59.20	2.30	10.1	220.0	16.9	10.7	17.9	0.01	0.04	16.2
CB-4 ^c	37.00	200.0	1.60	34.5	818.0	28.3	5.20	11.8	0.02	0.11	25.2
CB-5 ^c	29.40	72.90	2.10	10.5	238.0	31.1	38.8	18.2	0.00	0.04	18.4
CB-6 ^c	28.90	59.60	1.90	10.2	216.0	27.2	12.0	19.7	0.04	0.03	16.6
CB-7 ^c	24.10	74.20	1.70	11.4	239.0	22.5	57.1	4.70	0.01*	0.03	24.9
CB-8 ^c	13.50	47.60	1.70	11.6	156.0	29.4	10.8	7.60	0.02	0.01	17.3
CB-9 ^c	34.00	87.90	1.90	14.0	351.0	21.9	23.5	13.7	0.15	0.05	19.2
CB-10 ^c	37.90	81.20	2.30	15.2	337.0	29.2	10.1	12.9	0.35	0.04	17.0
CB-11 ^c	21.40	39.60	1.50	6.90	131.0	17.5	24.4	11.4	0.01	0.05	13.3
CB-12 ^c	10.00	9.800	2.20	3.10	31.40	18.9	18.5	0.60	0.12	0.05	18.4
CB-13 ^c	11.20	11.10	2.60	2.90	50.00	10.3	6.80	1.50	0.03	0.05	23.5
CB-14 ^c	10.30	10.30	2.30	2.60	49.10	3.80	4.80	0.70	0.02	0.07	20.2
CB-15 ^c	9.600	5.100	1.40	1.60	27.20	6.00	8.50	1.80	0.04	0.05	13.6
CB-16 ^c	111.7	310.0	2.30	22.6	1214	21.5	0.06*	13.4	7.15	0.11	46.2
CB-17 ^c	283.3	480.0	10.6	41.6	2147	21.3	0.06*	18.3	2.30	0.09	44.4
CB-18 ^c	280.0	330.0	20.3	38.9	2024	31.3	0.40	21.9	2.29	0.08	45.0
CB-19 ^c	124.2	330.0	4.40	36.6	1249	13.2	0.04	6.20	9.67	0.15	38.0
CB-20 ^c	305.9	517.0	11.3	45.6	2358	22.2	0.03	19.2	7.02	0.14	43.8
GB-1 ^d	91.90	376.0	2.70	40.2	1579	14.1	0.09*	12.3	0.01	0.02*	132
GB-2 ^d	17.30	27.80	8.40	22.9	255.0	1.30	6.60	7.10	0.05	0.01*	80.2
GB-3 ^d	31.70	59.00	7.20	28.8	381.0	2.60	0.09*	13.1	0.03	0.02*	77.0
GB-4 ^d	48.90	361.0	16.8	12.2	1246	5.10	0.09*	15.4	0.02	0.02*	79.6
GB-5 ^d	44.60	191.0	3.90	31.1	849.0	8.00	0.09*	15.0	0.02	0.02*	80.7

Table 2 continued

	Na	Ca	K	Mg	HCO ₃	Cl	NO ₃	SO ₄	Fe	Al	Si
GB-6 ^d	25.00	113.0	2.00	30.6	572.0	4.80	0.09*	22.7	0.01	0.01*	69.3
GB-7 ^d	89.50	279.0	4.10	68.4	1407	7.50	0.09*	11.2	0.01	0.01*	70.6
GB-8 ^d	13.20	235.0	24.6	56.3	1053	6.50	0.10*	14.8	0.01	0.01*	87.5
GB-9 ^d	81.60	286.0	2.60	56.3	1354	6.70	0.10*	17.1	0.01	0.01*	52.6
GB-10 ^d	10.90	241.0	0.80	14.8	779.0	6.40	0.10*	15.0	0.01*	0.01*	47.3
GB-11 ^d	36.00	355.0	16.8	37.6	1358	8.80	0.09*	8.00	0.02	0.01*	76.4
GB-12 ^d	97.00	521.0	4.70	87.1	2263	8.60	0.09*	14.0	0.01	0.01*	90.1
GB-13 ^d	86.00	400.0	4.50	54.0	1624	8.30	0.09*	31.5	0.01*	0.01*	53.1
GB-14 ^d	41.80	146.3	2.70	31.0	663.0	21.3	0.08*	38.4	0.00	0.03	40.2

*Imputed value

^aChoi et al. (2005)

^bYun and Kim (2000)

^cJeong et al. (2001)

^dJeong (2002)

(Palarea-Albaladejo and Martín-Fernández 2015). This algorithm provides a method of estimating values below the detection limit while preserving the relative structure of the data.

Geochemical modeling

Geochemical modeling was performed using PHREEQC (Parkhurst and Appelo 1999, 2013) with the Lawrence Livermore Laboratory (LLNL) database. Biotite, which is not included in the LLNL database, was added by the command PHASES, and its solubility constant ($\log K$) of -12.55 and enthalpy (ΔH) of 22 kJ/mol were used (Palandri and Kharaka 2004). Plagioclase was replaced by albite and anorthite (Choi et al. 2014; Gaus et al. 2005). To simulate the evolution of carbonate water, we formulated a hypothesis that the carbonate water originated from interactions between magmatic CO₂, deep groundwater, and bedrock-forming minerals, and then the carbonate water moved up to the shallow groundwater aquifer along various geological structures (faults and fractures), finally resulting in the generation of CSW through a diverse range of processes including mixing, dilution, and water–rock interactions (Fig. 2). Based on this hypothesis, the evolutionary pathway of carbonate water in the deep environment as well as the formation of CSW was simulated by EPM in the PHREEQC code. EPM is considered to be a powerful tool for estimating aqueous phase concentrations of

many elements using their saturation indices, which are included in the LLNL database. To simulate the primary stage for the generation of carbonate water in the deep bedrock aquifer, the deep groundwater was assumed to be meteoric water that has permeated into the deep bedrock aquifer under high CO₂ conditions (Koh et al. 2000; Yun and Kim 2000; Choi et al. 2014). As the meteoric water moved into the deep environment, water–rock interactions might be enhanced due to the increase in the residence time and geothermal gradient. As a result, the meteoric water would change to groundwater with high ionic concentration. Choi et al. (2005) conducted a study to estimate the temperature at which the carbonate water was formed and reported a range of 100 – 251 °C. In the present study, the temperature for the generation of carbonate water was assumed to be 150 °C. The redox potential was also an important parameter in the simulation, with 70 mV ($pe = -0.833$) assumed here based on the result provided by Koh et al. (2000). Another key parameter influencing the formation of carbonate water is the partial pressure of CO₂ (P_{CO_2}) originating from magmatic gases. Schaller et al. (2012) reported the P_{CO_2} values of lavas erupted from numerous volcanoes with a maximum value of 4500 ± 1200 ppm; therefore, a CO₂ concentration of 4500 ppm (0.102 mol/kg of water) was used in this study. All the simulations were conducted with the assumptions of a pressure of 1 atm and water density and mass of 1 g/cm³ and 1 kg, respectively. A full set

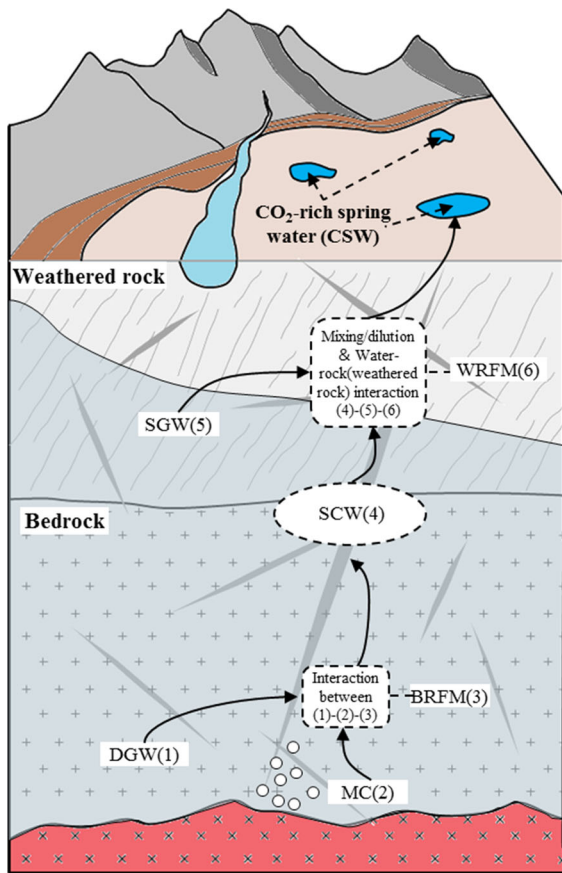


Fig. 2 Conceptual diagram showing the geochemical evolution of CO₂-rich spring water (CSW). *DGW* deep groundwater, *MC* magmatic CO₂, *BRFM* bedrock-forming mineral, *SCW* simulated carbonate water, *SGW* shallow groundwater, and *WRFM* weathered rock-forming mineral

of simulation parameters for each area is given in Table 3. The simulation of CSW formation was conducted by stepwise sequences. First, the evolution of carbonate water was simulated via interactions of magmatic CO₂ with deep groundwater and the bedrock-forming minerals listed in Table 3. Second, the formation of CSW was simulated by mixing between the modeled carbonate water and shallow groundwater with interactions with the minerals included in weathered rocks (Table 3). The mixing ratios were adjusted in nine steps from 1:9 to 9:1. Third, the simulations of each mixing ratio were iterated 25 times with the change of temperature ranging from the average measured value of each CSW (16.8, 16.6, and 14.0 °C for the KW, CB, and GB areas, respectively) to 150 °C. Accordingly, 225

runs were undertaken for the simulations of each area. Finally, by comparing the hydrochemical properties between the simulated and real CSWs, the most relevant mixing ratio and temperature were obtained.

Results and discussion

Water chemistry of CSW

The hydrochemical data of CSW used in this study are given in Tables 1 and 2. Based on the concentrations of the major ionic species, the hydrochemical facies of CSW in each area were analyzed using Piper plots (Fig. 3). Most CSWs were of the Ca–HCO₃ type, but Na–HCO₃-type CSWs were observed in five sites in the KW province. The Na–HCO₃ type CSWs have a higher Na, K, and Si content than the Ca–HCO₃ type CSWs, whereas the Ca–HCO₃-type CSWs have higher Ca, Mg, and Fe concentrations (Table 2). This indicates that the Na–HCO₃-type CSWs have undergone more severe silicate weathering processes than the Ca–HCO₃-type CSWs (Choi et al. 2014). Despite their convenience, traditional Piper plots make meaningful interpretations about hydrochemical evolution difficult because of a messy arrangement of overlapping data (Owen et al. 2016). To compensate for this drawback of conventional Piper plots (Fig. 3), ternary principal components plots were prepared using CodaPack (Fig. 4). Figure 4 condenses the compositional variability into a descriptive tool for identifying the water types of CSW for each area based on the relationships between the relative proportions of major constituents (Owen et al. 2016). Overall, the CSW was much more affected by PC1 than by PC2. More specifically, 87% of the CSW seemed to be influenced dominantly by the behavior of Ca and Mg (PC1), while 13% of the CSW was characterized by Ca and Na + K (PC2) (Fig. 4a). On the other hand, 85% of the CSW appeared to be affected by Ca and HCO₃ (PC1) and 15% was characterized by HCO₃ and Cl (PC2), as shown in Fig. 4b. Using the relative proportions of K–Si–Fe shown in Fig. 4c, the relative effects of K-feldspar (Si–K, PC1) and biotite (Si–Fe, PC2) were interpreted. Most (95%) of the CSW tended to be influenced by PC1, while only 5% of the CSW was more likely affected by PC2. Finally, it was confirmed that 87 and 13% of the CSW were

Table 3 Conditions of equilibrium phases modeling for the simulation of geochemical evolution of CO₂-rich spring water (CSW)

Study area	pH	pe	Temperature (°C)		Al	HCO ₃	Ca	Fe	K (mg/L)	Mg	Na	SO ₄	Si
			Deep groundwater	Shallow groundwater									
Back-ground groundwater	6.37	- 0.83	150	16.77	0.001	18.67	3.43	0.200	0.57	0.930	4.170	2.23	14.47
Kangwon (KW) ^a													
Chungbuk (CB) ^b	6.38	- 0.83	150	16.62	0.038	83.05	24.6	0.011	1.77	4.920	15.72	10.03	15.53
Gyeongbuk (GB) ^c	7.00	- 0.83	150	14.00	0.183	272.4	53.5	0.105	3.00	16.50	25.90	3.000	33.00
Kangwon (KW)													
Chungbuk (CB)													
Gyeongbuk (GB)													
Bedrock ^a													
Weathered rock													
Mineral	Conc. (moles)	Ca-HCO ₃ type		Na-HCO ₃ type ^d		Weathered rock		Bedrock ^f		Weathered rock ^g			
		Mineral	Conc. (moles)	Mineral	Conc. (moles)	Mineral	Conc. (moles)	Mineral	Conc. (moles)	Mineral	Conc. (moles)	Mineral	Conc. (moles)
Albite	10.1	Albite	10.09	Albite	14.6	Albite	7.83	Albite	7.83	Albite	9.16	Albite	4.70
Anorthite	4.39	Anorthite	4.39	Anorthite	0.86	Anorthite	7.38	Anorthite	7.38	Anorthite	8.64	Anorthite	4.43
Biotite	0.95	Biotite	0.95	Diopside	0.43	Biotite	1.55	Biotite	1.55	Biotite	3.21	K-feldspar	2.02
CO ₂ (g)	0.10	Hematite	1.89	Enstatite	0.06	CO ₂ (g)	0.10	K-feldspar	10.2	CO ₂ (g)	0.10	Muscovite	0.16
Hematite	1.89	K-feldspar	8.34	Ferrosilite	0.07	K-feldspar	10.2	Kaolinite	0.00	K-feldspar	4.42	Quartz	60.0
K-feldspar	8.34	Kaolinite	0.00	K-feldspar	10.4	Muscovite	0.43	Muscovite	0.43	Pargasite	0.04		
Quartz	60.04	Muscovite	0.00	Magnetite	0.57	Quartz	49.3	Quartz	49.3	Quartz	50.2		
		Quartz	60.04	Quartz	54.1					Clinochlore- ^{7A}	0.11		

^aChoi et al. (2014)^bYun and Kim (2000)^cKoh et al. (2000)^dMin and Kim (1996)^eKoh et al. (2008)^fLee and Lee (1991)^gJeong and Jeong (1999)

Fig. 3 Piper diagram showing the hydrochemical facies of CO₂-rich spring water (CSW) in each study area

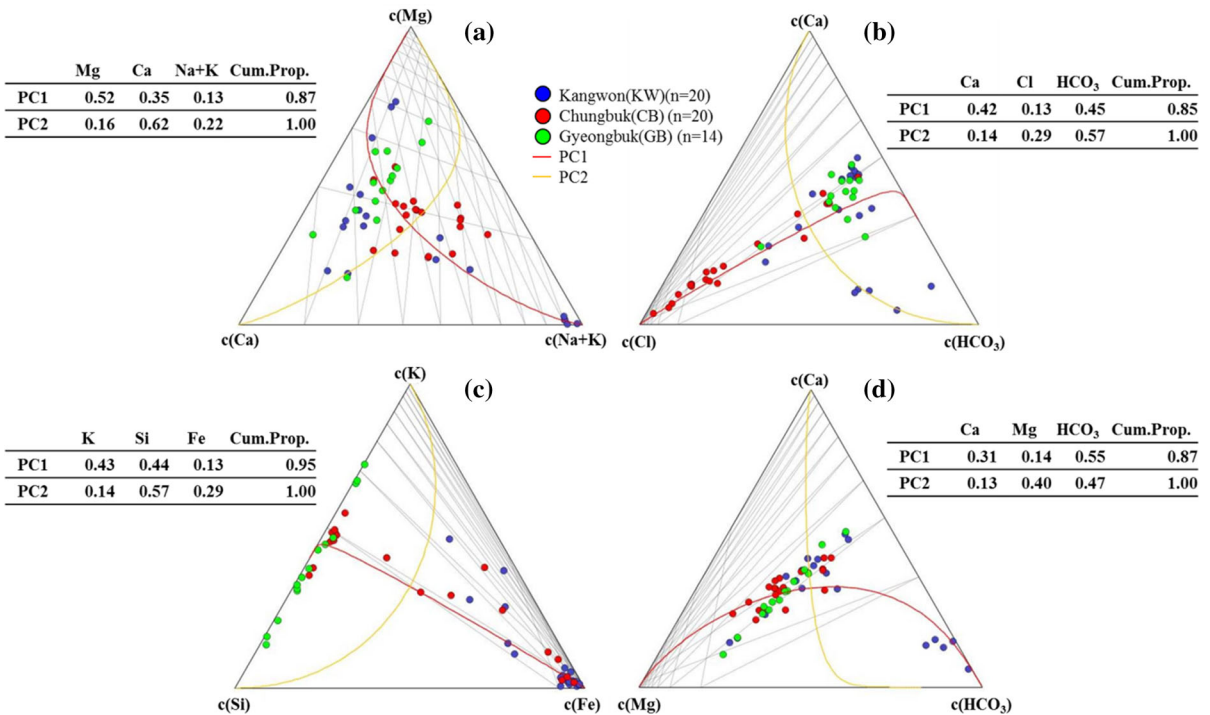
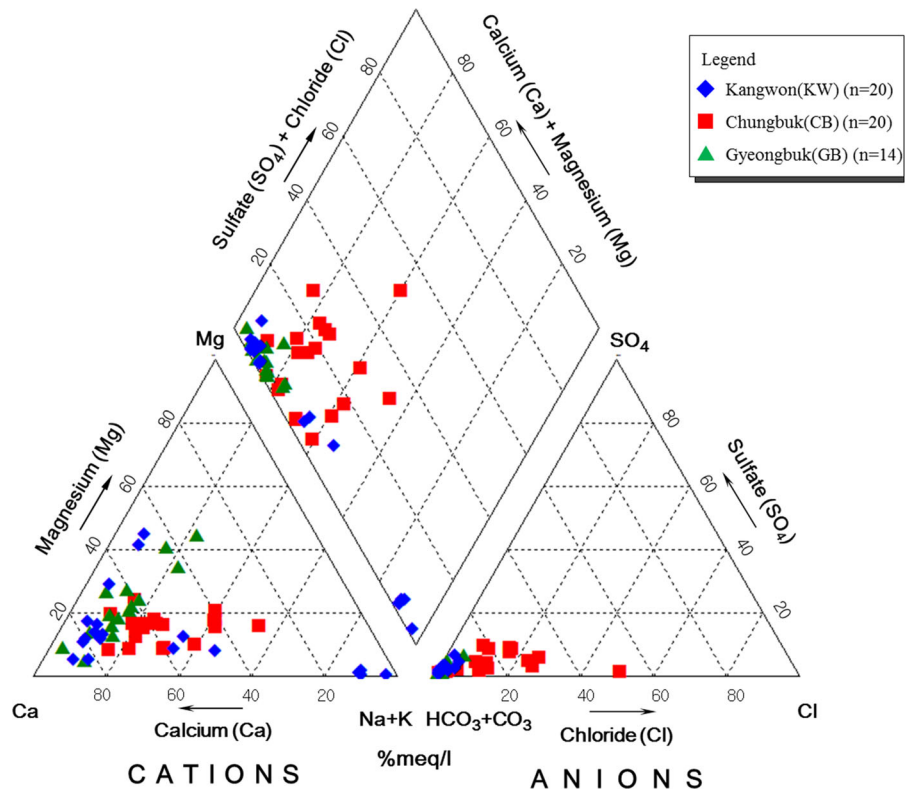


Fig. 4 Ternary principal components plot. **a** Mg–Ca–Na + K, **b** Ca–Cl–HCO₃, **c** K–Si–Fe and **d** Ca–Mg–HCO₃

characterized as Ca–HCO₃ and Mg–HCO₃ types, respectively (Fig. 4d).

To delineate the effect of water–rock interactions on the hydrochemical properties of the CSW, the relationship between molar ratios of major elements and TDS and HCO₃ is presented in Fig. 5. First, the relative effects of albite and anorthite were elucidated using the molar ratio of Na and Ca (Fig. 5a). The lower ratios indicated that most of the CSW seemed to be affected by anorthite, except for five samples from the KW area of Na–HCO₃ type. Comparing the relative effects of albite and K-feldspar using the molar ratio of K and Na (Fig. 5b), the CSW was more influenced by albite than by K-feldspar, except for one sample in the GB area. A significantly lower ratio of Si/Al was observed in most of the CSW (Fig. 5c), indicating that dissolution of primary minerals was dominant in most of the CSW. To examine the source of Fe, the molar ratios of Fe/SO₄ were investigated (Fig. 5d). Most of the CSW from the KW area exhibited a relatively high molar ratio of Fe/SO₄, indicating that these CSWs were predominantly affected by primary minerals bearing Fe or secondary minerals such as hematite, rather than pyrite. As shown in Fig. 4d, the effect of Ca was more dominant than that of Mg (Fig. 5e). Lastly, the relatively low ratios of Ca/HCO₃ (Fig. 5f) indicate that the CSW likely originated from magmatic evolution rather than the interactions with carbonate minerals.

Results of compositional data analyses

The CSW within each area was classified statistically and interpreted using R, CodaPack, and SPSS programs. First, the R package zCompositions was used for imputation of values below the detection limit of compositional data based on the methodology proposed by Palarea-Albaladejo and Martín-Fernández (2015). The results of the imputation are given in Table 2. After the imputation, principal component analyses (PCA) were conducted using the CodaPack program. The clr biplots obtained from the PCA are presented in Fig. 6. The PCA results show that constituents such as Si, SO₄, Mg, Cl, and H were distributed in the first component (PC1) with positive values, whereas others such as K, Na, HCO₃, Ca, Fe, and Al had negative values on PC1. Additionally, the constituents with positive PC1 values were dominant in the CB and GB areas, but those with negative PC1

values appeared in the KW and in part of the CB area. Furthermore, the CSW of the CB area appeared to have positive PC1 and negative PC2 values, the CSW samples in the GB area dominantly had positive PC1 and PC2 components, and the CSW of the KW area tended to have negative PC1 and PC2 values. The reason why the density of the clr biplot was different between areas can be explained easily by the data shown in Table 2. It was confirmed that the constituents having the largest Euclidean distance from the center were Fe, NO₃, and Mg (Fig. 6): their concentrations were much higher than those of other constituents. A hierarchical cluster analysis (HCA) was applied to classify the CSW according to area. Prior to the HCA, the ilrs of proportions of major ions derived from an intuitive sequential binary partition (SBP) were used to characterize the hydrochemical variability within and between the areas. There are two methods for developing a SBP: by experience and by PCA (Pawlowsky-Glahn and Egozcue 2011). In this study, the SBP was derived using the Euclidean distance of PCA (Table 4). Figure 7 presents an ilr dendrogram acquired from the SBP of CodaPack and explains the different behaviors of constituents in each area. In the CB area, a significant difference was not observed between the two groups of constituents (K, Na, and HCO₃ vs. Ca, Al, and Fe). However, the K, Na, and HCO₃ group was more dominant than that of Ca, Al, and Fe in the GB area, and vice versa in the KW area. Additionally, the effects of Mg, H, and NO₃ were more dominant than those of Si, Cl, and SO₄ in the CB area, but the tendency was the opposite in the GB and KW areas. Overall, the CSW of the GB area was more affected by Si, Cl, SO₄, Mg, H, and NO₃ than by K, Na, HCO₃, Ca, Al, and Fe, but the opposite was true in the KW area. However, no significant difference was observed in the CB area. Using the ilr coordinates derived from the SBP, a HCA was conducted using SPSS (Fig. 8). The CSW was classified into five groups. The first cluster (C1) is characterized by having a lower concentration of Fe and a higher concentration of NO₃, indicating that it was likely produced in a relatively shallow aquifer that had a relatively high recharge rate or was vulnerable to pollution. The second cluster (C2) tended to have lower concentrations of Fe and NO₃ and may have formed in a shallow environment with a relatively low recharge. The CSW of the third cluster (C3) was characterized by higher Fe concentration and lower Al

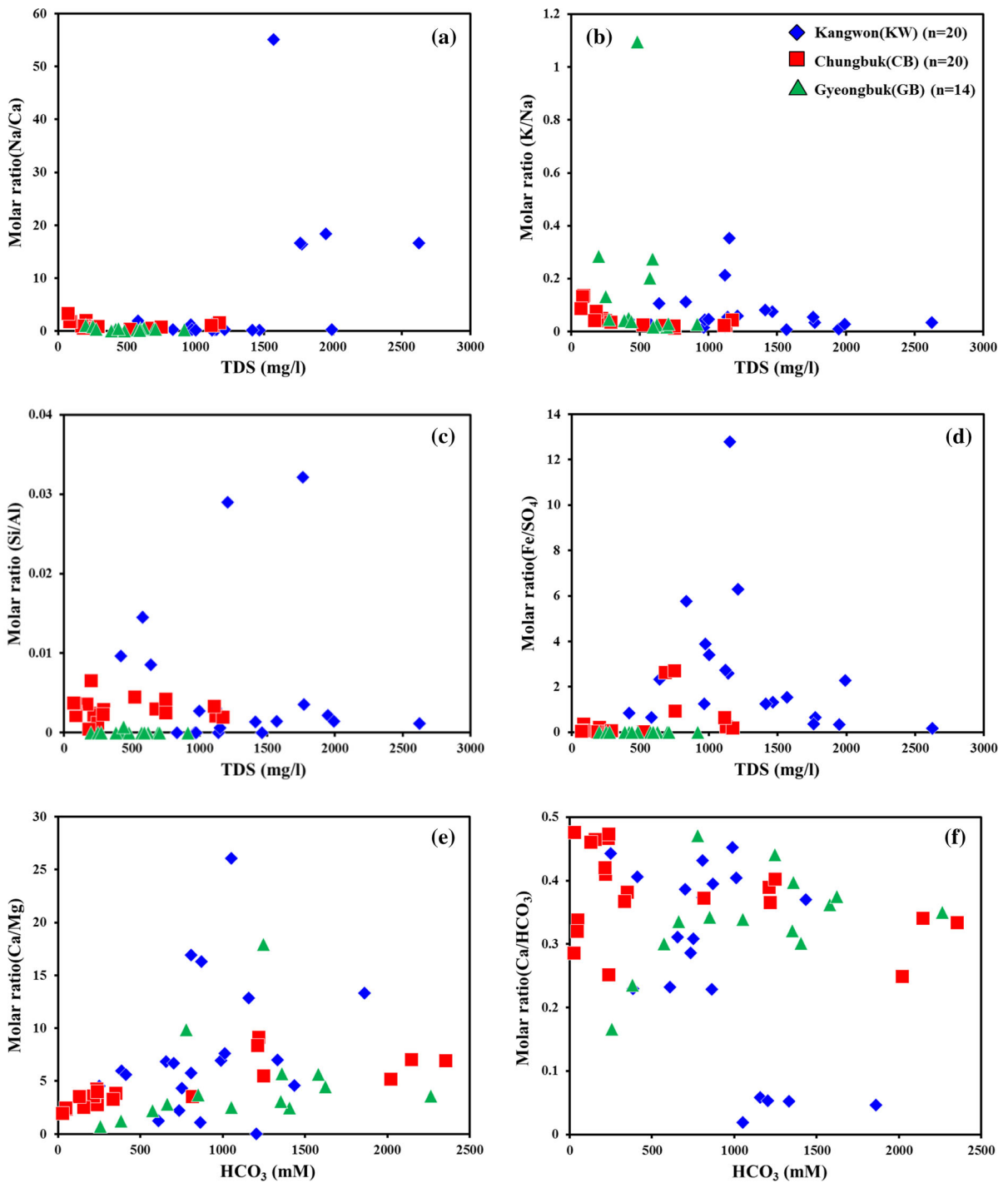


Fig. 5 Schematic diagrams showing the relationships between molar ratios of major elements and TDS/ HCO_3^- of CO_2 -rich spring water (CSW) in each study area. **a** Molar ratio (Na/Ca) versus TDS. **b** Molar ratio (K/Na) versus TDS. **c** Molar ratio (Si/

Al) versus TDS. **d** Molar ratio (Fe/SO₄) versus TDS. **e** Molar ratio (Ca/Mg) versus HCO_3^- . **f** Molar ratio (Ca/HCO₃) versus HCO_3^-

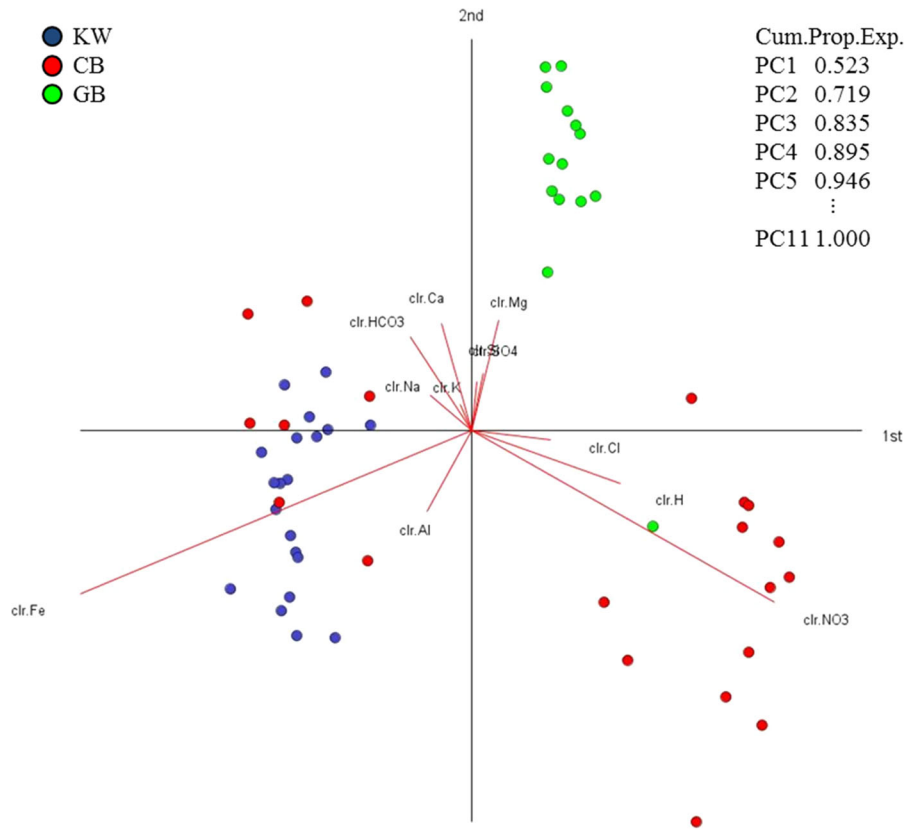


Fig. 6 A centered-log ratio (clr) biplot of data set for each study area. Cum.Prop.Exp = cumulative proportion of explained variance

Table 4 Sequential binary partition (SBP) of a 11-part composition (x_1, x_2, \dots, x_{11}) for describing isometric log ratio (ilr) coordinates for the hierarchical cluster analysis (HCA)

Balance	NO ₃	H	Mg	SO ₄	Cl	Si	Fe	Al	Ca	HCO ₃	Na	K
X ₁	+	+	+	+	+	+	-	-	-	-	-	-
X ₂	+	+	+	-	-	-						
X ₃	+	+	-									
X ₄	+	-										
X ₅				+	+							
X ₆				+	-							
X ₇							+	+	+	-	-	-
X ₈							+	+	-			
X ₉							+	-				
X ₁₀										+	+	-
X ₁₁										+	-	

content, indicating that it was influenced by Fe-bearing minerals, such as hematite. The fourth cluster (C4) was Na–HCO₃ type CSW. Finally, the CSW of the fifth cluster (C5) was likely affected by Fe-bearing silicate minerals, such as biotite, because of the relatively high concentrations of Fe and Al. Based

on the HCA results, the proportions of CSW samples in each cluster are listed in Table 5. C1 encompassed 13 and 1 CSW samples from the CB and GB areas, respectively. Most of the CSW samples in the GB area appeared to belong to C2. Clusters C3 and C4 included only 5 CSW samples from the KW area. Finally, C5

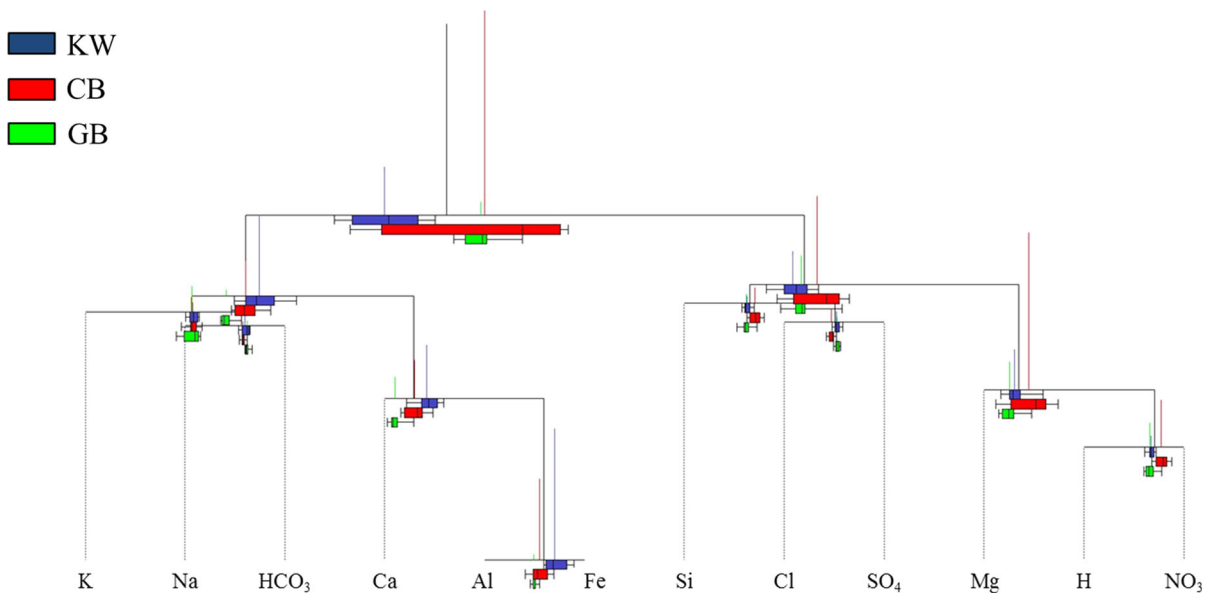


Fig. 7 Balance dendrogram showing distinctions in the isometric log ratio (ilr) as defined in Table 4

was composed of 10 and 7 CSW samples from the KW and CB areas, respectively, which seemed to have been affected by biotite in the granite and metamorphic rocks that are distributed in those two areas. Consequently, the HCA conducted via calculation of clr and ilr revealed the structural variability of the CSW in each area, and the characteristics of water–rock interactions, external effects, and formation environments could be inferred from the HCA results.

Simulation of the geochemical evolution of CSW using equilibrium phase modeling

The geochemical evolution of CSW was simulated using EPM incorporated in the PHREEQC code, and the results are presented in Figs. 9, 10 and 11. As mentioned in “Geochemical modeling,” the evolution of CSW was simulated by a stepwise method. The first step was to simulate the formation of carbonate water in the deep environment as a result of the interaction between deep groundwater–magmatic–rock-forming minerals (Fig. 2), and the CSW was then generated via the geochemical processes of mixing between the simulated carbonate water and shallow groundwaters, and water–rock interaction. Accordingly, EPM was conducted to simulate the evolutionary stage of CSW just before it occurs on the surface. The simulated CSW is hereafter referred to as SCSW, to distinguish

simulated results from field CSW data. The model lines on each graph shown in Figs. 9, 10, and 11 were obtained by connecting the lines acquired by simulation with different mixing ratios between the simulated carbonate water and shallow groundwater. For the simulation of each mixing ratio, the temperature was changed from 150 °C for simulation of deep carbonate water to the average values of each CSW (e.g., 16.8, 16.6, and 14.0 °C for the KW, CB, and GB areas). In this way, the final properties of the SCSW were similar to those of the real CSW. In the case of the KW area, two kinds of CSW (Ca–HCO₃ and Na–HCO₃ types) occurred and the simulations were conducted twice to compute each type of CSW. In the simulation for the Ca–HCO₃-type CSW, the best fit was obtained at a temperature of 77.8 °C. On the other hand, the best simulation results were obtained at 150 °C for the Na–HCO₃-type CSW. In the cases of the CB and GB areas, the best results were acquired at temperatures of 138.9 and 93.0 °C, respectively. A larger amount of albite was simulated to be dissolved at higher temperature, resulting in an increase in Na concentration. However, Ca concentration increased at lower temperature due to the dissolution of anorthite. By contrast, the concentrations of K, Mg, and Si were not likely to be affected by temperature. Hence, the relative proportion of Ca and Na can be used as an

Fig. 8 Dendrogram showing the hierarchical cluster analysis (HCA) of CO₂-rich spring water (CSW)

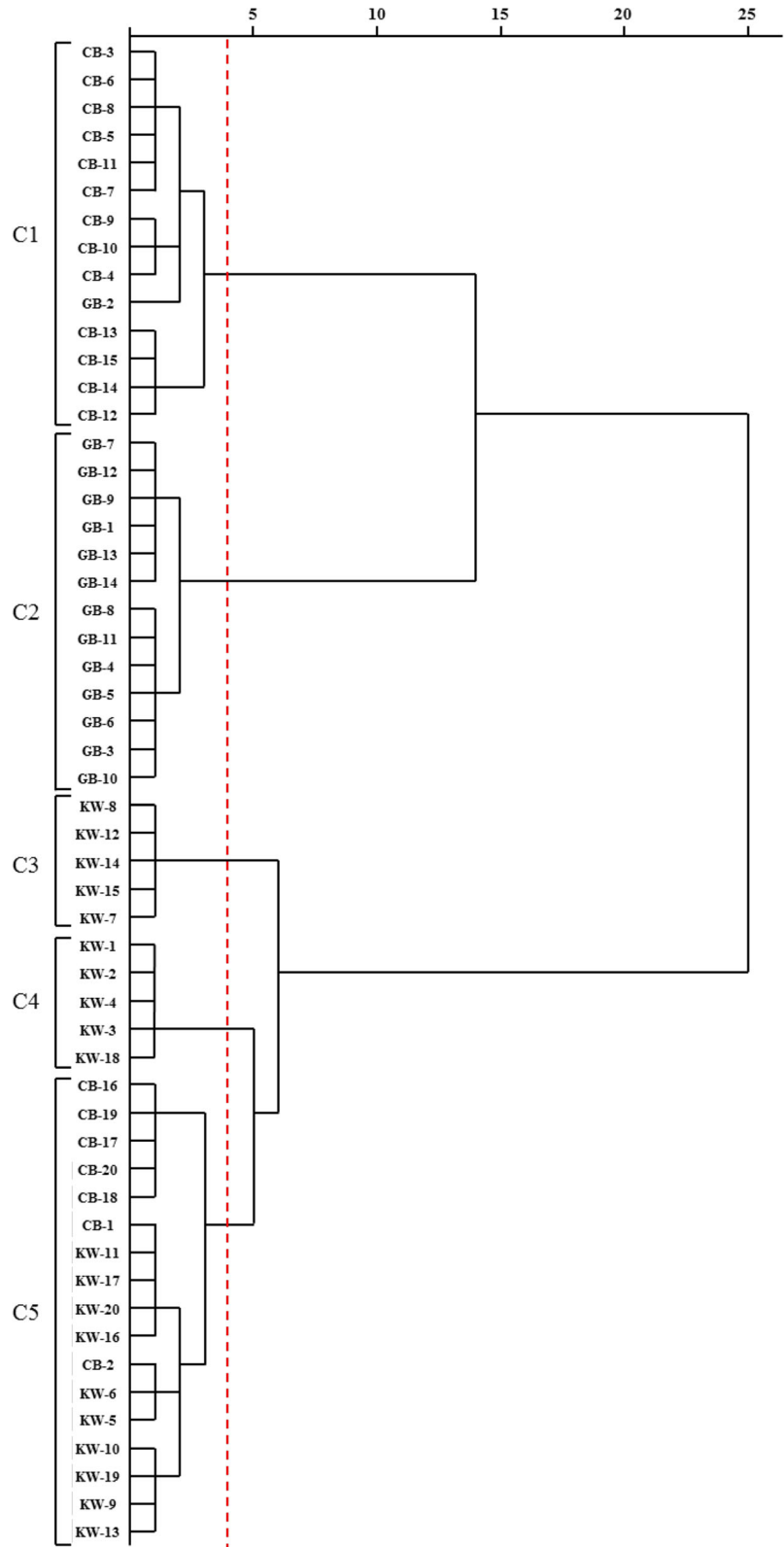


Table 5 HCA results showing the CSW distribution of each area in five clusters

Area	C ₁	C ₂	C ₃	C ₄	C ₅
KW	–	–	5	5	10
CB	13	–	–	–	7
GB	1	13	–	–	–

indicator to infer the depth of CSW formation because temperature can be directly linked to depth.

The simulation results indicate that the depth of carbonate water formation increased with increasing temperature. However, as the carbonate water moved up along the various geological structures, it mixed with shallow groundwater and the temperature gradually changed. In addition to the temperature drop, water–rock interactions have taken place continuously. As a result, the water quality changed significantly and then approached equilibrium with increasing residence time. However, according to Koh and Chae (2008), the residence time of the CSW occurring within the study area was relatively short (15–50 years), indicating that the chemistry of the CSW might not have established a state of equilibrium. However, our simulations were conducted using the EPM of the PHREEQC code, and a state of equilibrium was assumed. For this reason, the water chemistry of the SCSW tended to deviate from that of the real CSW, as confirmed by the simulation results shown in Figs. 9, 10 and 11. The equilibrium state and formation temperature of each CSW could be estimated using the concentration ratio between Na, K, and Mg (Giggenbach 1988). A discrimination diagram is shown in Fig. 12, obtained by the method suggested by Giggenbach (1988). The Na–HCO₃-type CSW of five sites within the KW area appeared to be equilibrated, but the other CSWs did not approach equilibrium. Additionally, based on the formation temperature shown in the discrimination diagram (Fig. 12), it can be speculated that the Na–HCO₃-type CSW was formed at a relatively higher temperature range (100–230 °C). This indicates that the formation environment was deep and also that the residence time of this CSW was longer. As a result, the possibility of approaching the equilibrium state increased. Based on the simulation results (Figs. 9, 10, 11), the concentrations of K and Mg appeared to be different between the

SCSW and the real CSW, which might be attributed to the difference in the degree of equilibrium state.

When the geochemical evolution of CSW was investigated by modeling, the mixing ratios between simulated carbonate water and shallow groundwater were adjusted. In the case of the Ca–HCO₃-type CSWs occurring in the KW and GB areas, the simulation results were obtained by changing the mixing ratio between simulated carbonate water and shallow groundwater from 1:9 to 9:1. Mixing ratios of 1:9–5:5 were simulated for the Na–HCO₃-type CSW of the KW area, while mixing ratios of 1:9–3:7 were used for the simulation of the CB area, resulting in a relatively smaller contribution of carbonate water. The results indicate that the CSW in this area was formed by the small amount of carbonate water in the deep environment or the large amount of shallow groundwater. These simulation results could be related to the results of the compositional data analyses. As shown in Table 5 and Fig. 8, the CSW was categorized into five groups. As mentioned in “Results of compositional data analyses,” the CSW belonging to C1 was characterized as having a lower concentration of Fe and a higher concentration of NO₃, which indicates that these CSWs were produced in a relatively shallow aquifer with a high recharge. This is supported by the simulation results showing mixing ratios of 1:9–3:7, indicating a greater effect of shallow groundwater. On the other hand, the results of the compositional data analyses indicate that C2 which contained most of the CSW in the GB area was generated in a shallower aquifer with a lower recharge. This is supported by the simulation results in which mixing ratios of 1:9–9:1 were relevant, suggesting that the CSW of the GB area was affected more by carbonate water than by shallow groundwater.

This study proposed a schematic, but relatively simple methodology to simulate the formation of carbonate water in a deep environment and the geochemical evolution of CSW. By estimating the temperature of the groundwater system in each area, the depth of carbonate water formation may be calculated, because the formation temperature of carbonate waters can be speculated from the results of the study. Additionally, it was demonstrated that the behavior of various minerals can be evaluated via a simulation of the mixing of carbonate water with shallow groundwater, together with an interpretation of water–rock interactions.

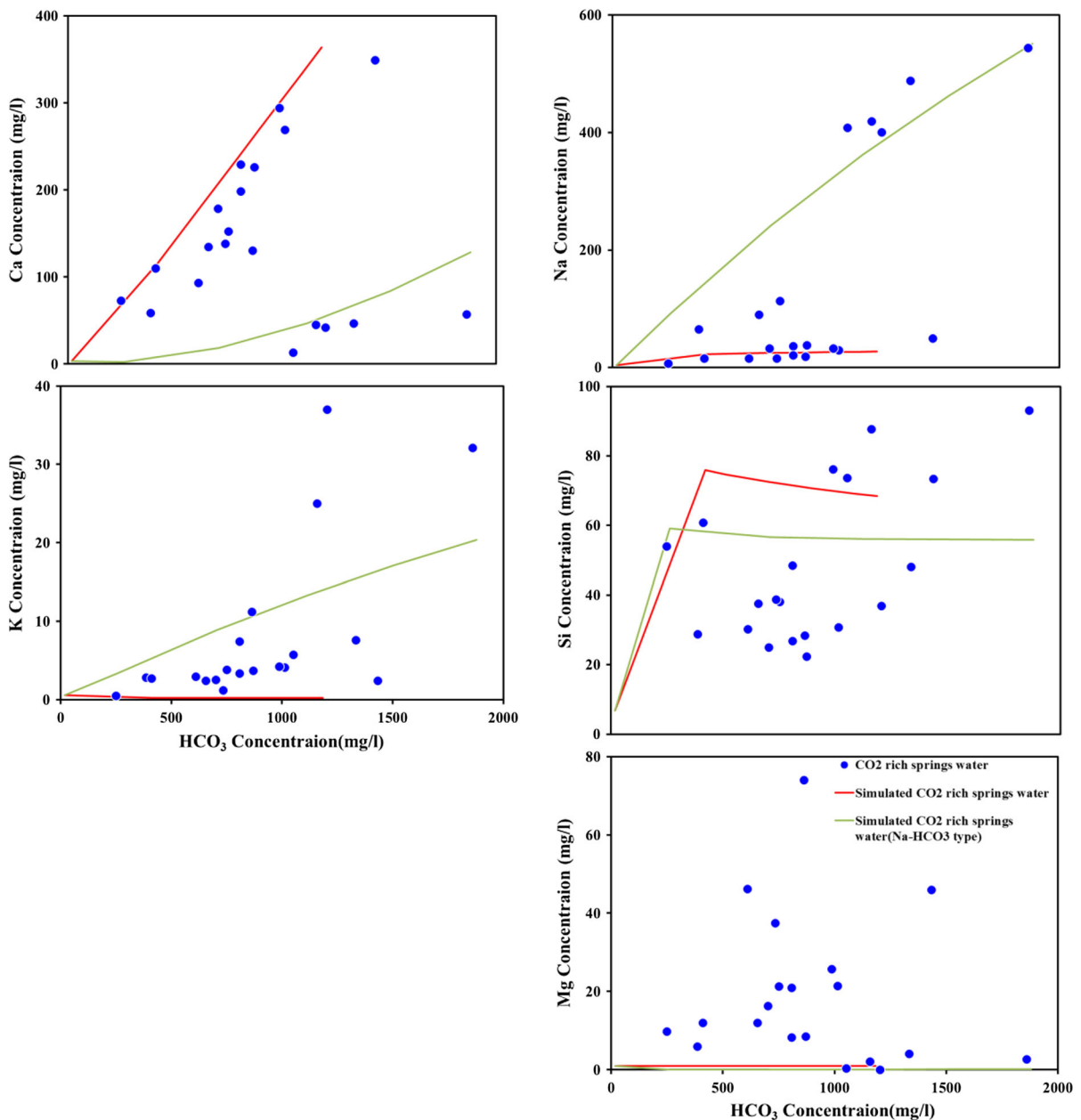


Fig. 9 Simulation results for geochemical evolution of CO₂-rich spring water (CSW) in Kangwon (KW) area

Conclusions

There are three typical areas of naturally outflowing CSW in South Korea. This study was initiated to compare the hydrochemical properties of CSWs between areas and to classify them on the basis of any similarity in their chemistry. Only 5 CSW samples of the KW area were classified as Na-HCO₃ type

water; the other samples were Ca-HCO₃ water type. Using the ternary principal components plot, the relative effects between major constituents on the properties of the CSW were delineated. Additionally, the CSW within the study area was classified to five groups via HCA analyses. The CSW of C1 was characterized as being formed in a shallower aquifer with a high recharge; most of the CSW in the CB area

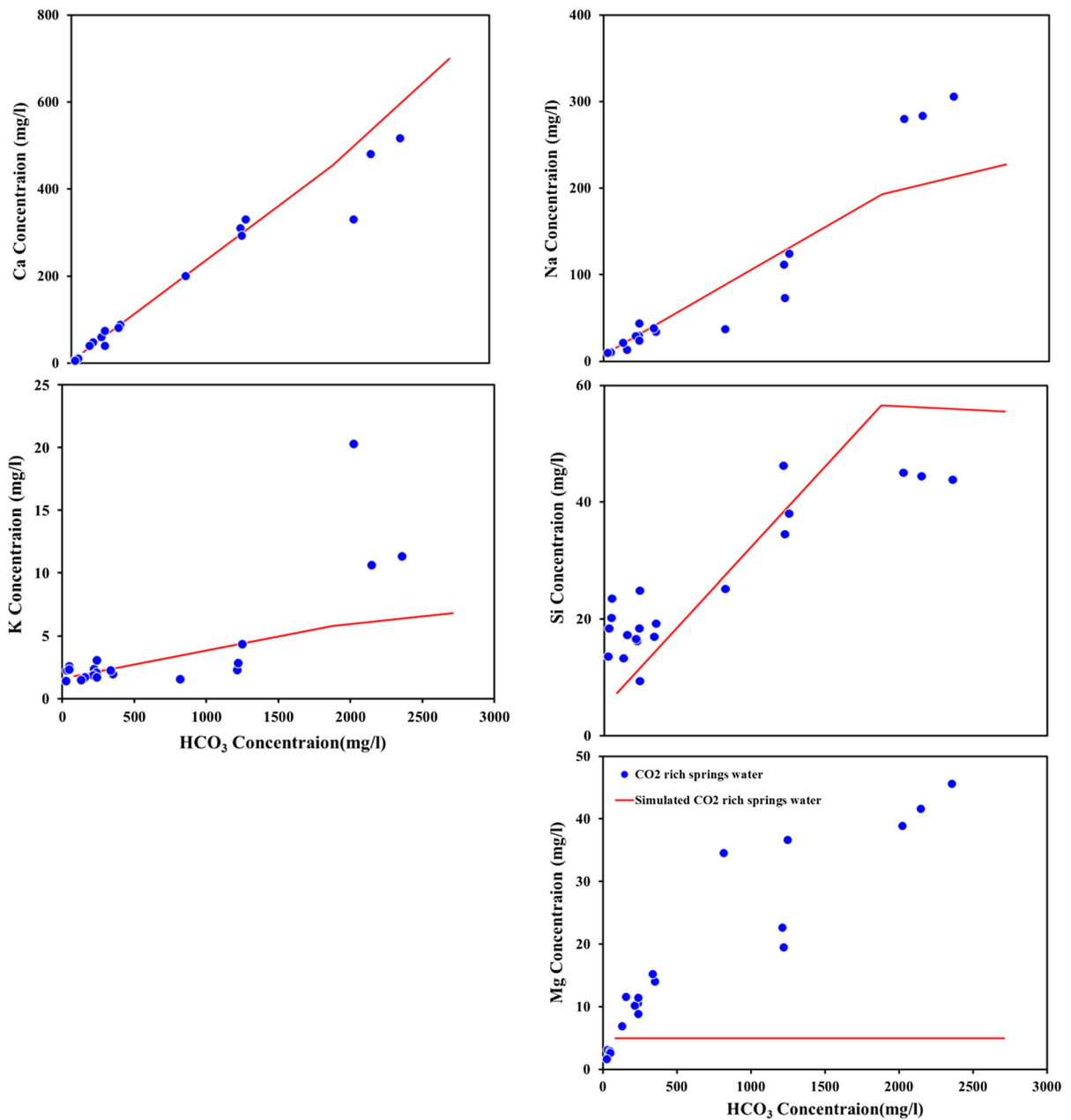


Fig. 10 Simulation results for geochemical evolution of CO₂-rich spring water (CSW) in Chungbuk (CB) area

belonged to this group. Group C2, encompassing the CSW of the GB area, was speculated to have formed in a shallower environment with a lower recharge. The C3 group of CSW seemed to be greatly affected by Fe-bearing minerals, and only five samples of the KW area were included in this group. The CSW of the C4 group was Na–HCO₃-type water and included only five samples from the KW area. Finally, group C5 was

characterized as being affected by Fe-bearing silicate minerals, such as the biotite in granite and metamorphic rocks. This group was composed of 10 and 7 CSW samples from the KW and CB areas, respectively.

In addition to multivariate statistical analyses, we simulated the geochemical evolution of CSW using EPM. The simulation was conducted using stepwise

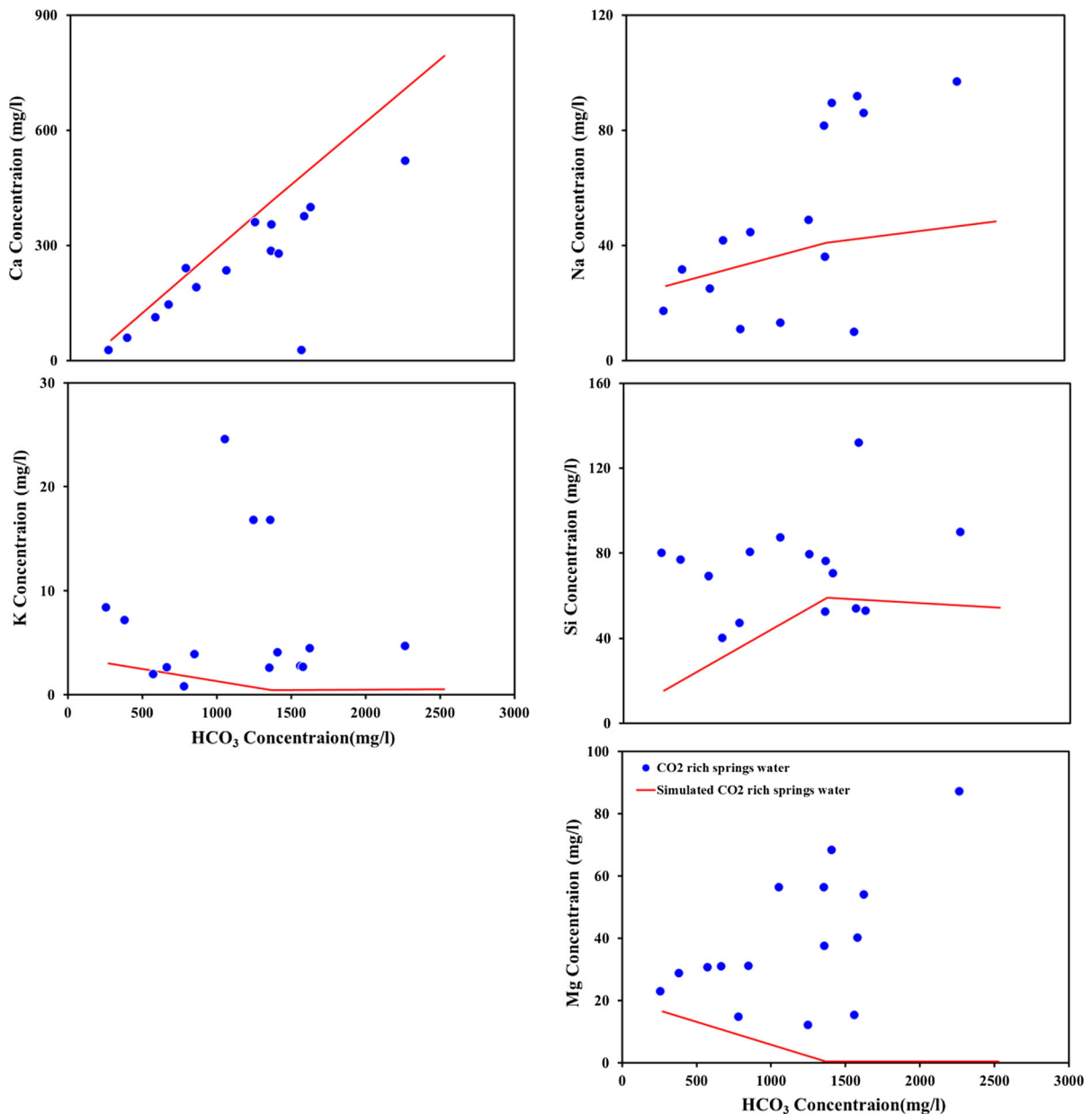
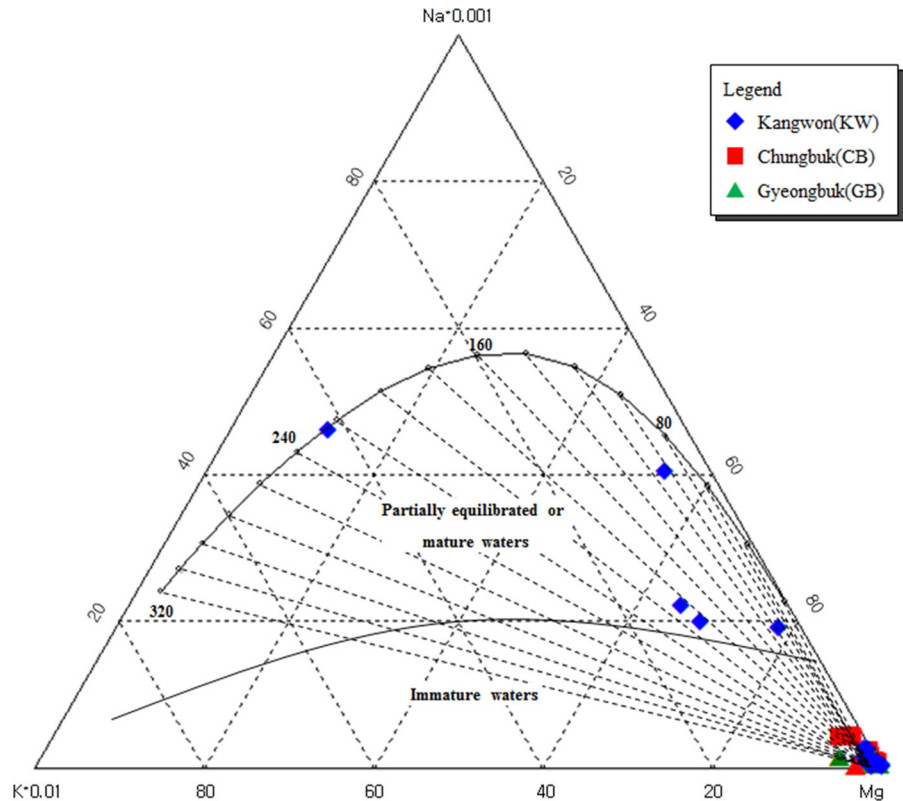


Fig. 11 Simulation results for geochemical evolution of CO₂-rich spring water (CSW) in Gyeongbuk (GB) area

approaches. First, we simulated the carbonate water originating from a deep environment through interactions among magmatic CO₂, deep groundwater, and bedrock-forming minerals. Next, the geochemical evolution of CSW was estimated via the simulation of geochemical processes, including mixing between carbonate water and shallow groundwater and water–rock interactions taking place in a shallow environment. To acquire the best simulation results, modeling

conditions, such as the mixing ratios between the simulated carbonate water and shallow groundwater, temperature, and rock-forming minerals, were adjusted according to the area of concern. Generally, the chemistry of simulated CSW was similar to that of real CSW. However, the simulated composition of some elements, such as K and Mg, was somewhat different from the real values, which might be attributed to the difference in the degree of

Fig. 12 Giggenbach discrimination diagram to estimate the equilibrium state and formation temperature of carbonate water



equilibrium state between simulated and real systems. Based on the simulation results, the Na–HCO₃-type CSW was interpreted to be formed at a higher temperature range than the Ca–HCO₃ type CSW, indicating that the formation environment of Na–HCO₃ type CSW was deeper. Furthermore, the simulation results suggest that the relative contribution of carbonate water in producing CSW could be estimated according to the areas of concern. Additionally, the simulation results on the mixing ratios between carbonate water and shallow groundwater and CSW formation temperature were intimately related to the HCA results, particularly for groups C1 and C2.

The significant contributions of the present study were (1) the methodology proposed could be effectively applied to studies investigating CSW distributed over extensive areas, (2) CSW chemistry could be simulated using equilibrium phase modeling and the formation temperature and depth of CSW could be estimated through modeling, with adjustment of the diverse range of temperatures of the system, and (3) the chief factors affecting the geochemical evolution

of CSW from carbonate water originating in deep environments could be determined through modeling. Consequently, the methodology used in this study could be applied to predict the behavior of CO₂ after its geological storage, as well as to evaluate the stability and security of geologically stored CO₂.

Acknowledgements This research was supported by “R&D project on Environmental Management of Geologic CO₂ Storage” from the KEITI (Project No. 2014001810001) and partially supported by the Basic Research Program (GP2017-027) of the Korea Institute of Geoscience and Mineral Resources (KIGAM).

References

Aitchison, J. (1986). *The statistical analysis of compositional data*. London, U. K.: Chapman and Hall.
 Akin, T., Guney, A., & Kargi, H. (2015). Modeling of calcite scaling and estimation of gas breakout depth in a geothermal well by using PHREEQC. In *Proceedings of the fortieth workshop on geothermal reservoir engineering*. Stanford University, Stanford, CA, January 26–28.
 Bacon-Shone, J. (2006). A short history of compositional data analysis. In V. Pawlowsky-Glahn & A. Buccianti (Eds.),

- Compositional data analysis: Theory and applications* (Vol. 378). Chichester: Wiley.
- Balashov, V. N., Guthrie, G. D., Hakala, J. A., Lopano, C. L., Rimstidt, J. D., & Brantley, S. L. (2013). Predictive modeling of CO₂ sequestration in deep saline reservoirs: Impacts of geochemical kinetics. *Applied Geochemistry*, 30, 41–56.
- Balashov, V. N., Guthrie, G. D., Lopano, C. L., Hakala, J. A., & Brantley, S. L. (2015). Reaction and diffusion at the reservoir/shale interface during CO₂ storage: Impact of geochemical kinetics. *Applied Geochemistry*, 61, 119–131.
- Belkhir, L., Boudoukha, A., Mouni, L., & Baouz, T. (2010). Application of multivariate statistical methods and inverse geochemical modeling for characterization of groundwater—A case study: Ain Azel plain (Algeria). *Geoderma*, 159, 390–398.
- Blake, S., Henry, T., Murray, J., Flood, R., Muller, M. R., Jones, A. G., et al. (2016). Compositional multivariate statistical analysis of thermal groundwater provenance: A hydrogeochemical case study from Ireland. *Applied Geochemistry*, 75, 171–188.
- Bollengier, O., Choukroun, M., Grasset, O., Menn, E. L., Bellino, G., Morizet, Y., et al. (2013). Phase equilibria in the H₂O–CO₂ system between 250–330 K and 0–1.7 GPa: Stability of the CO₂ hydrates and H₂O–ice VI at CO₂ saturation. *Geochimica Cosmochimica Acta*, 119, 322–339.
- Bong, L. S., & Chung, G. S. (2000). Diagenetic history of Ordovician Chongson limestone in the Chongson area, Kangwon province, Korea. *Journal of the Korean Earth Science Society*, 21, 449–468 (in Korean with English abstract).
- Buccianti, A., & Zuo, R. (2016). Weathering reactions and isometric log-ratio coordinates: Do they speak to each other? *Applied Geochemistry*, 75, 189–199.
- Chae, G. T., Jo, M., Kim, J. C., & Yum, B. W. (2013). Geochemical study on CO₂-rich waters of Daepyeong area, Korea: Monitoring implication for CO₂ geological storage. *Energy Procedia*, 37, 4366–4373.
- Choi, H. S., Koh, K. Y., Bae, D. S., Park, S. S., Hutcheon, I., & Yun, S. T. (2005). Estimation of deep-reservoir temperature of CO₂-rich springs in Kangwon district, South Korea. *Journal of Volcanology and Geothermal Research*, 141, 77–89.
- Choi, H. S., Koh, Y. K., Kim, C. S., Bae, D. S., & Yun, S. T. (2000). Environmental isotope characteristics of CO₂-rich water in the Kangwon province. *Journal of Korean Society of Economic and Environmental Geology*, 33, 491–504.
- Choi, H. S., Koh, Y. K., Yun, S. T., & Kim, C. S. (2002). Geochemical study on the mobility of dissolved elements by rocks–CO₂-rich waters interaction in the Kangwon province. *Economic and Environmental Geology*, 35, 533–544 (in Korean with English abstract).
- Choi, B. Y., Yun, S. T., Kim, K. H., Choi, H. S., Chae, G. T., & Lee, P. K. (2014). Geochemical modeling of CO₂-water-rock interactions for two different hydrochemical types of CO₂-rich springs in Kangwon District, Korea. *Journal of Geochemical Exploration*, 144, 49–62.
- Choi, H. S., Yun, S. T., Koh, Y. K., Mayer, B., Park, S. S., & Hutcheon, I. (2009). Geochemical behavior of rare earth elements during the evolution of CO₂-rich groundwater: A study from the Kangwon district, South Korea. *Chemical Geology*, 262, 318–327.
- Choi, B. Y., Yun, S. T., Mayer, B., Hong, S. Y., Kim, K. H., & Jo, H. Y. (2012). Hydrogeochemical processes in clastic sedimentary rocks, South Korea: A natural analogue study of the role of dedolomitization in geologic carbon storage. *Chemical Geology*, 306–307, 103–113.
- Chopping, C., & Kaszuba, J. P. (2012). Supercritical carbon dioxide–brine–rock interactions in the Madison Limestone of Southwest Wyoming: An experimental investigation of a sulfur-rich natural carbon dioxide reservoir. *Chemical Geology*, 322–323, 223–236.
- Egozcue, J. J., & Pawlowsky-Glahn, V. (2005). Groups of parts and their balances in compositional data analysis. *Mathematical Geology*, 37, 795–828.
- Egozcue, J. J., Pawlowsky-Glahn, V., Mateu-Figueras, G., & Barceló-Vidal, C. (2003). Isometric logratio transformations for compositional data analysis. *Mathematical Geology*, 35, 279–300.
- Evans, M. J., & Derry, L. A. (2002). Quartz control of high germanium/silicon ratios in geothermal waters. *Geology*, 30, 1019–1022.
- Fačevicová, K., Bábek, O., Hron, K., & Kumpan, T. (2016). Element chemostratigraphy of the Devonian/Carboniferous boundary: A compositional approach. *Applied Geochemistry*, 75, 211–221.
- Filzmoser, P., Hron, K., & Tolosana-Delgado, R. (2016). Statistical analysis of geochemical compositions: Problems, perspectives and solutions. *Applied Geochemistry*, 75, 169–170.
- Flaathen, T. K., Gislason, S. R., Oelkers, E. H., & Sveinbjörnsdóttir, Á. E. (2009). Chemical evolution of the Mt. Hekla, Iceland, groundwaters: A natural analogue for CO₂ sequestration in basaltic rocks. *Applied Geochemistry*, 24, 463–474.
- García-Ríos, M., Cama, J., Luquot, L., & Soler, J. M. (2014). Interaction between CO₂-rich sulfate solutions and carbonate reservoir rocks from atmospheric to supercritical CO₂ conditions: Experiments and modeling. *Chemical Geology*, 383, 107–122.
- Gaus, I. (2010). Role and impact of CO₂-rock interactions during CO₂ storage in sedimentary rocks. *International Journal of Greenhouse Gas Control*, 4, 73–89.
- Gaus, I., Azaroual, M., & Czernichowski-Lauriol, I. (2005). Reactive transport modeling of the impact of CO₂ injection on the clayey cap rock at Sleipner (North Sea). *Chemical Geology*, 17, 319–337.
- Giggenbach, W. F. (1988). Geothermal solute equilibria. Derivation of Na–K–Mg–Ca geothermometers. *Geochimica Cosmochimica Acta*, 48, 2693–2711.
- Hwang, J. Y., Choi, J. B., Jeong, G. Y., Oh, J. H., Choi, Y. H., & Lee, J. H. (2013). Occurrence and mineralogical characteristics of dolomite ores from South Korea. *Journal of the Mineralogical Society of Korea*, 26, 87–99 (in Korean with English abstract).
- Jeong, C. H. (2002). Genesis and hydrochemistry of CO₂-rich spring from Kyungpook province, Korea. *Economic and Environmental Geology*, 35, 121–136 (in Korean with English abstract).
- Jeong, C. H. (2004). Hydrochemistry and formation environment of CO₂-rich springs from the Kangwon province.

- Journal of the Mineralogical Society of Korea*, 17, 61–73 (in Korean with English abstract).
- Jeong, C. H., & Jeong, G. Y. (1999). Geochemical water quality and genesis of carbonated dalki mineral water in the Chungson area, Kyungpook. *Economic and Environmental Geology*, 32, 455–468 (in Korean with English abstract).
- Jeong, C. H., Kim, J. G., & Lee, J. Y. (2001). Occurrence, geochemistry and origin of CO₂-rich water from the Chungcheong area, Korea. *Economic and Environmental Geology*, 34, 227–241 (in Korean with English abstract).
- Jeong, C. H., Kim, H. J., & Lee, S. Y. (2005). Hydrochemistry and genesis of CO₂-rich springs from Mesozoic granitoids and their adjacent rocks in South Korea. *Geochemical Journal*, 39, 517–530.
- Jeong, C. H., & Lee, J. K. (2000). Geochemistry and origin of CO₂-rich groundwater from sedimentary rocks of Kyungsang system. *The Journal of Engineering Geology*, 10, 51–62 (in Korean with English abstract).
- Jeong, C. H., Yoo, S. W., Kim, K. H., & Nagao, K. (2011). Hydrochemistry and origin of noble gases and CO₂ gas within carbonated mineral waters in the Kyeoungbuk-Kangwon province, Korea. *The Journal of Engineering Geology*, 21, 65–77 (in Korean with English abstract).
- Jin, J., Zimmerman, A. R., Martin, J. B., & Khadka, M. B. (2015). Spatiotemporal variations in carbon dynamics during a low flow period in a carbonate karst watershed: Santa Fe River, Florida, USA. *Biogeochemistry*, 122, 131–150.
- Kharaka, Y. K., Cole, D. R., Thordsen, J. J., Kakouros, E., & Nance, H. S. (2006). Gas–water–rock interactions in sedimentary basins: CO₂ sequestration in the Frio Formation, Texas, USA. *Journal of Geochemical Exploration*, 89, 183–186.
- Kharitonova, N. A., Chelnokov, G. A., Vakh, E. A., Karabtsov, A. A., & Zykin, N. N. (2010). Geochemistry of carbonate mineral water from the Fadeevskoe deposit of the Primorye region. *Russian Journal of Pacific Geology*, 4, 78–90.
- Kim, K., Jeong, D. H., Koh, Y. K., Kim, S. H., & Park, E. (2008). The geochemical evolution of very dilute CO₂-rich water in Chungcheong Province, Korea: Processes and pathways. *Geofluids*, 8, 3–15.
- Kim, G. Y., Koh, Y. K., Bae, D. S., Kim, C. S., & Park, M. E. (2001). Geochemistry and isotope studies of the Shinchon CO₂-rich waters in the Gyeongsang province. *Economic and Environmental Geology*, 34, 71–88 (in Korean with English abstract).
- Kim, G. Y., Koh, Y. K., Choi, H. S., Kim, C. S., & Bae, D. S. (2000). Mineralogy and geochemistry of carbonate precipitates from CO₂-rich water in the Jungwon area. *Journal of the Mineralogical Society of Korea*, 13, 22–36 (in Korean with English abstract).
- Koh, D. C., & Chae, G. T. (2008). Estimation of mixing properties and mean residence time using ³H for groundwater in typical geothermal and CO₂-rich areas in South Korea. *Journal of the Geological Society of Korea*, 44, 507–522 (in Korean with English abstract).
- Koh, Y. K., Choi, B. Y., Yun, S. T., Choi, H. S., Mayer, B., & Ryoo, H. S. (2008). Origin and evolution of two contrasting thermal groundwaters (CO₂-rich and alkaline) in the Jungwon area, South Korea: Hydrochemical and isotopic evidence. *Journal of Volcanology and Geothermal Research*, 178, 777–786.
- Koh, Y. K., Kim, C. S., Bae, D. S., & Lee, D. I. (2000). Hydrochemistry and environmental isotope studies of the deep groundwater in the Munkyeong area. *Economic and Environmental Geology*, 33, 469–489 (in Korean with English abstract).
- Koh, Y. K., Yun, S. T., Kim, C. S., Choi, H. S., & Kim, G. Y. (1999). Geochemical evolution of CO₂-rich groundwater in the Jungwon area. *Economic and Environmental Geology*, 32, 469–483 (in Korean with English abstract).
- Ledesma-Ruiz, R., Pasten-Zatata, E., Parra, R., Harter, T., & Mahlknecht, J. (2015). Investigation of the geochemical evolution of groundwater under agricultural land: A case study in northeastern Mexico. *Journal of Hydrology*, 521, 410–423.
- Lee, J. I., & Lee, M. S. (1991). Mineralogy and petrology on the granitic rock in the Youngju area, Kyungsang buk-do. *Journal of the Geological Society of Korea*, 27, 626–641 (in Korean with English abstract).
- Lee, N. K., Oh, S. J., Kang, B. K., & Noh, J. H. (2003). Occurrence and ore types of high-Ca limestone from the pungchon formation. *Korean Association of Human Resource Development*, 17, 101–111 (in Korean with English abstract).
- Lu, H. Y., Lin, C. K., Lin, W., Liou, T. S., Chen, W. F., & Chang, P. Y. (2011). A natural analogue for CO₂ mineral sequestration in Miocene basalt in the Kuanhsi-Chutung area, Northwestern Taiwan. *International Journal of Greenhouse Gas Control*, 5, 1329–1338.
- Manning, C., Shock, E. L., & Sverjensky, D. A. (2013). The chemistry of carbon in aqueous fluids at crustal and upper-mantle conditions: Experimental and theoretical constraints. *Reviews in Mineralogy and Geochemistry*, 75, 109–148.
- Martos-Rosillo, S., & Moral, F. (2015). Hydrochemical changes due to intensive use of groundwater in the carbonate aquifers of Sierra de Estepa (Seville, Southern Spain). *Journal of Hydrology*, 528, 249–263.
- Min, K. W., & Kim, S. B. (1996). Geochemistry and petrogenesis of the granitic rocks in the vicinity of th Mt. Sorak. *The Journal of the Petrological Society of Korea*, 5, 35–51 (in Korean with English abstract).
- Moore, J., Adams, M., Allis, R., Lutz, S., & Rauzi, S. (2005). Mineralogical and geochemical consequences of the long-term presence of CO₂ in natural reservoirs: an example from the Springerville—St. Johns Field, Arizona, and New Mexico, USA. *Chemical Geology*, 217, 365–385.
- Noh, J. H., Oh, S. J., & Kim, K. J. (2004). Applied-mineralogical study on the mineral facies and characteristics of domestic high-Ca limestone. *The Journal of Engineering Geology*, 17, 339–355 (in Korean with English abstract).
- Nyirenda, T. M., Zhou, J., Xie, L., Pan, X., & Li, Y. (2015). Determination of carbonate minerals responsible for alkaline mine drainage at Xikuangshan Antimony Mine, China: Using thermodynamic chemical equilibrium model. *Journal of Earth Science*, 26, 755–762.
- Owen, D. D. R., Pawlowsky-Glahn, V., Egozcue, J. J., Buccianti, A., & Bradd, J. M. (2016). Compositional data analysis as a robust tool to delineate hydrochemical facies

- within and between gas-bearing aquifers. *Water Resource Research*, 52, 5771–5793.
- Palandri, J. L., & Kharaka Y. K. (2004). *A compilation of rate parameters of water–mineral interaction kinetics for application to geochemical modeling*. Open File Report 2004-1068, US Geological Survey.
- Palarea-Albaladejo, J., & Martín-Fernández, J. A. (2015). zCompositions—R package for multivariate imputation of left-censored data under a compositional approach. *Chemosometrics and Intelligent Laboratory Systems*, 143, 85–96.
- Parkhurst, D. L., & Appelo, C. A. J. (1999). *User's guide to PHREEQC (ver.2)—A computer program for speciation, batch-reaction, one-dimensional transport, and inverse geochemical calculations*. U.S. Geol. Survey, Water Resources Investigation, Report 99-4259.
- Parkhurst, D. L., & Appelo, C. A. J. (2013). *Description of input and examples for PHREEQC version 3—A computer program for speciation, batch-reaction, one-dimensional transport, and inverse geochemical calculations*. U.S. Geological Survey, Techniques and Methods, Book 6, Chap. A43.
- Pauwels, H., Gaus, I., le Nindre, Y. M., Pearce, J., & Czernichowski-Lauriol, I. (2007). Chemistry of fluids from a natural analogue for a geological CO₂ storage site (Montmiral, France): lessons for CO₂–water–rock interaction assessment and monitoring. *Applied Geochemistry*, 22, 2817–2833.
- Pawlowsky-Glahn, V., & Egozcue, J. J. (2006). Compositional data and their analysis: An introduction. *Geological Society London Special Publications*, 264, 1–10.
- Pawlowsky-Glahn, V., & Egozcue, J. J. (2011). Exploring compositional data with the coda-dendrogram. *Austrian Journal of Statistics*, 40, 103–113.
- Pearce, J. M. (2006). What can we learn from natural analogues? An overview of how analogues can benefit the geological storage of CO₂. In S. Lombardi, L. K. Altunina, & S. E. Beaubien (Eds.), *Advances in the geological storage of carbon dioxide*. NATO science series (Vol. 65, pp. 129–138). Berlin: Springer.
- Pearson, K. (1896). Mathematical contributions to the theory of evolution: On a form of spurious correlation which may arise when indices are used in the measurement of organs. *Proceedings of the Royal Society of London*, 60, 489–498.
- Rafighdoust, Y., Eckstein, Y., Harami, R. M., Gharaie, M. H. M., & Mahboubi, A. (2016). Using inverse modeling and hierarchical cluster analysis for hydrochemical characterization of springs and Talkhab River in Tang-Bijar oilfield, Iran. *Arabian Journal of Geosciences*, 9, 241–253.
- Raju, N. J., Patel, P., Gurung, D., Ram, P., Gossel, W., & Wycisk, P. (2015). Geochemical assessment of groundwater quality in the Dun valley of central Nepal using chemometric method and geochemical modeling. *Groundwater for Sustainable Development*, 1, 135–145.
- Ryzhenko, B. N., & Cherkasova, E. V. (2012). Chemical composition of natural waters and brines as a result of hydrogeochemical processes in water–rock–gas systems. *Geochemistry International*, 50, 1101–1150.
- Sanchez, D., Barbera, J. A., Mudarra, M., & Andreo, B. (2015). Hydrogeochemical tools applied to the study of carbonate aquifers: Examples from some karst systems of Southern Spain. *Environmental Earth Sciences*, 74, 199–215.
- Schaller, M. F., Wright, J. D., Kent, D. V., & Olsen, P. E. (2012). Rapid emplacement of the central atlantic magmatic province as a net sink for CO₂. *Earth Planetary Science Letters*, 323, 27–39.
- Sharif, M. U., Davis, R. K., Steele, K. F., Kim, B., & Kresse, T. M. (2008). Inverse geochemical modeling of groundwater evolution with emphasis on arsenic in the Mississippi River Valley alluvial aquifer, Arkansas (USA). *Journal of Hydrology*, 350, 41–55.
- Springer, R. D., Wang, Z., Anderko, A., Wang, P., & Felmy, A. R. (2012). A thermodynamic model for predicting mineral reactivity in supercritical carbon dioxide: I. Phase behavior of carbon dioxide–water–chloride salt systems across the H₂O-rich to the CO₂-rich regions. *Chemical Geology*, 322–323, 151–171.
- Tallini, M., Falcone, R. A., Carucci, V., Falgiani, A., Parisse, B., & Petitta, M. (2014). Isotope hydrology and geochemical modeling: new insights into the recharge processes and water–rock interactions of a fissured carbonate aquifer (Gran Sasso, central Italy). *Environmental Earth Sciences*, 72, 4957–4971.
- Tolosana-Delgado, R., & McKinley, J. (2016). Exploring the joint compositional variability of major components and trace elements in the Tellus soil geochemistry survey (Northern Ireland). *Applied Geochemistry*, 75, 236–276.
- Watson, M. N., Zwingmann, N., & Lemon, N. M. (2004). The Ladbroke Grove-Katnook carbon dioxide natural laboratory: A recent CO₂ accumulation in a lithic sandstone reservoir. *Energy*, 29, 1457–1466.
- White, W. B. (1997). Thermodynamic equilibrium, kinetics, activation barriers, and reaction mechanisms for chemical reactions in Karst Terrains. *Environmental Geology*, 30, 46–58.
- Wickham, H. (2009). *ggplot2: Elegant graphics for data analysis*. New York, NY: Springer.
- Yun, J. A., & Kim, K. H. (2000). Geochemistry and stable isotopes of carbonate waters in South Korea. *The Journal of Korean Society of Soil and Groundwater Environment*, 7, 116–124 (in Korean with English abstract).
- Yun, H. S., Park, D. W., Lee, B. D., & Hong, S. S. (2003). Occurrence, physical and petrochemical properties of the marbles by geological ages in South Korea. *The Journal of Engineering Geology*, 13, 429–444 (in Korean with English abstract).
- Zanini, L., Novakowski, K. S., Lapcevic, P., Bickerton, G. S., Voralek, J., & Talbot, C. (2000). Ground water flow in a fractured carbonate aquifer inferred from combined hydrogeological and geochemical measurements. *Ground Water*, 38, 350–360.